

Heat transfer and pressure drop characteristics of alternating clockwise and counter clockwise twisted tape inserts in the transitional flow regime

SM Abolarin, M Everts and JP Meyer*

Department of Mechanical and Aeronautical Engineering, University of Pretoria, Pretoria, 0002, South Africa.

*Author for correspondence, e-mail: josua.meyer@up.ac.za

13Dec2018

Abstract

The purpose of this study was to experimentally investigate the heat transfer and pressure drop characteristics in a smooth circular tube with alternating clockwise and counter clockwise twisted tape (CCCTT) inserts. The CCCTT inserts were fabricated from copper plate strips with a length, width and thickness of 450 mm, 18 mm and 1 mm respectively. The strips were twisted to obtain a twist ratio of 5 and 12 strips were joined longitudinally so that a clockwise direction twisted tape insert was connected to a counter clockwise direction twisted tape. The assembling was at connection angles of 0° , 30° and 60° , to form CCCTT inserts with an overall length of 5.27 m. The CCCTT inserts were placed in a smooth circular copper tube with an inner diameter of 19 mm. Water was used as the test fluid and experiments were conducted at constant heat fluxes of 1.35, 2, 3 and 4 kW/m² between Reynolds numbers of 300 and 11 404. This covered the laminar, transitional and turbulent flow regimes. Specific attention was given to the identification of the transitional flow regime with the CCCTT inserts and the influence of the connection angle and heat flux on the transitional flow regime. It was found that both the start and the end of the transitional flow regime were influenced by the connection angle and the heat flux. When different connection angles were compared it was found that an increase in connection angle enhanced the heat transfer in the transitional flow regime. An increase in heat flux significantly enhanced the heat transfer in the laminar flow regime and delayed transition. Heat transfer and pressure drop correlations were developed to predict the experimental data in the laminar, transitional and turbulent regimes as a function Reynolds number, modified Grashof number and connection angle.

Keywords: transition; clockwise; counter clockwise; twisted; tape; insert; enhanced

Highlights

- Heat transfer and pressure drop in the transitional flow regime
- Experiments with clockwise and counter clockwise twisted tape inserts
- Tape connection angle enhanced heat transfer
- Start and end of transition depended on connection angle and heat flux
- Earlier transition with increased connection angle and decreased heat flux

Nomenclature

A	area
C_p	specific heat capacity at constant pressure
D	test section diameter
eb	energy balance error
f	friction factor
g	acceleration due to gravity
Gr^*	modified Grashof number
h	heat transfer coefficient
H	pitch of the twisted tape; axial distance for a 180° rotation in twist
I	current
j	Colburn j -factor
k	thermal conductivity of the fluid
L	length/laminar flow regime
$L_{\Delta P}$	pressure drop length
\dot{m}	mass flow rate
Nu	Nusselt number
P	pressure
Pr	Prandtl number
\dot{q}	heat flux
\dot{Q}	heat transfer rate
Re	Reynolds number
ΔRe	width of the transitional flow regime
T	temperature
V	voltage
W	tape width
x	axial position measured from tube inlet
y	twist ratio (H/W)

Greek symbol

β	thermal expansion coefficient
δ	thickness of the twisted tape insert
μ	dynamic viscosity
ρ	density
θ	connection angle
ν	kinematic viscosity

Subscripts

b	bulk
c	cross-sectional
cr	start of transitional flow regime
e	exit, electrical
h	heated length
i	inlet, inner
L	laminar
m	mean
P	pressure

<i>qt</i>	end of transitional flow regime
<i>R</i>	transition
<i>s</i>	surface
<i>T</i>	turbulent

Abbreviations

CTT	conventional twisted tape
CCCTT	clockwise and counter clockwise twisted tape
PUCTT	peripheral u-cut twisted tape

1. Introduction

The growing concerns for energy as a grand challenge has increased the need to improve the heat transfer performance of heat exchangers which are widely used in the residential-, commercial- and manufacturing sectors. Many heat transfer improvements are achieved by either active or passive techniques, or both [1-3]. Active techniques such as vibration of a fluid or surface, mechanical aids, jet impingement, electrostatic field, etc. require additional sources of external power [4]. Passive techniques, on the other hand, do not require external power. These techniques are usually more energy efficient and are easy to fabricate at low costs [5]. A well-known passive technique is the insertion of one or a combination of flow turbulators into a tube/channel passage. These turbulators include coatings and/or roughness on the inner surface of the tube/channel passage, wire and helical coil inserts, corrugated tubes [6-9], outer grooved cylinder and inner rotating cylinder [10, 11], helical and eccentric helical screw tape inserts [12-14], twisted tape inserts of different modifications [15-25], etc.

The twisted tape insert as a flow turbulator has been found in many cases to increase heat transfer performance [26-28], particularly at lower Reynolds numbers. In literature, twisted tape inserts have been modified to improve heat transfer and thermal efficiency compared to smooth tubes. The advantages of using a twisted tape insert over a smooth tube include a higher heat transfer rate, improved mixing of the test fluid across the cross-section of the tube [16, 29, 30] and a thinner boundary layer thickness [31, 32]. However, the use of twisted tape inserts is accompanied with higher pressure drop [33, 34], which led to increased research investigations to improve the thermal efficiency of heat exchangers. In an attempt to reduce the pressure drop, experiments have also been conducted using shorter lengths of twisted tape inserts [35-37].

A comprehensive literature review on twisted tape inserts indicated that previous studies concentrated mainly on the laminar flow regime for Reynolds numbers between 13 and 3 000 [2, 5, 15, 37-45] or the turbulent flow regime for Reynolds numbers greater than 3 000 [4, 29, 33, 46-51] and not specifically on the transitional flow regime [52-55]. Up to now, only Wongcharee and Eiamsa-ard [15] (in the laminar flow regime) and Eiamsa-ard and Promvongse [4] (in the turbulent flow regime), considered alternating clockwise and counter clockwise twisted tape (CCCTT) inserts.

In general, the insertion of twisted tapes in heat exchangers provides an opportunity to achieve heat transfer augmentation [43, 47]. As the transitional flow regime might be a good compromise between the laminar (low heat transfer coefficients and pressure drops) and turbulent (high heat transfer coefficients and pressure drops) flow regimes, more research should be conducted to determine the influence of twisted tape inserts in the transitional flow regime [56]. Meyer and Abolarin [57] were the first to specifically focus on the transitional flow regime using twisted tape inserts. They considered conventional twisted tape (CTT) inserts, twisted in one direction only, but at different twist ratios of 3, 4 and 5. A square-edged inlet was used and careful attention was given to the inlet as previous works [58-62] indicated that the inlet geometry and inlet turbulence levels can significantly influence the transition behaviour. Two different techniques to accurately identify the transitional flow regime were presented. The first technique made use of three straight lines (on a log-log scale) through the laminar, transitional and turbulent flow regimes. The two Reynolds numbers at the intersection points were considered as the start and end of the transitional flow regime. The second technique was to monitor the standard deviation of the temperature and pressure drop data, because the standard deviations were higher in the transitional flow regime than in the other flow regimes. It was found that the start and end of the transitional flow regime could be accurately determined by using the two techniques complementary to each other. Both

the start and the end of the transitional flow regime depended on the twist ratio and the heat flux applied and occurred earlier compared to that of the smooth tube. The study of Meyer and Abolarin [57] established the transitional flow regime with the simplest form of the twisted tape insert (which was the CTT insert), therefore it was decided to conduct experiments with a modification of the CTT insert. Therefore, the purpose of this study was to experimentally investigate the heat transfer and pressure drop characteristics of CCCTT inserts in a smooth circular tube. Specific attention was given to the identification of the transitional flow regime with the CCCTT inserts and the influence of the connection angle and heat flux on the transitional flow regime. The tapes had a twist ratio of $y = 5$ and were connected at connection angles of $\theta = 0^\circ, 30^\circ$ and 60° . Because the inlet geometry has an effect on transition, a square-edged inlet was used to complement the previous work of Meyer and Abolarin [57].

2. Experimental set-up

The experimental set-up that was used to conduct the heat transfer and pressure drop experiments has been described in detail by Meyer and Abolarin [57] and is therefore discussed very succinctly in this paper. The major components of the experimental set-up are numbered from (1) to (14) in Fig. 1.

The water in the 5 000 ℓ reservoir (1) was maintained at 20°C by connecting it to an external chiller unit (2) with a cooling capacity of 15 kW. An electronically-controlled positive displacement pump (3) was used to circulate the cold water. An accumulator (4) was installed after the pump to reduce flow pulsations [63, 64]. After the accumulator followed a bypass valve (5) and two valves in parallel, upstream of the two Coriolis flow meters (6). The Coriolis flow meter with a range of 4 – 108 ℓ/h was used for the mass flow rate measurements in the laminar and transitional flow

regimes, while the Coriolis flow meter with a range of 54 – 2 180 ℓ/h was used for higher mass flow rate measurements, mostly in the turbulent flow regime.

A calming section similar to the design of Ghajar and co-workers [59, 62] was installed upstream of the test section. The functions of the calming section were to eliminate flow disturbances and to ensure a uniform inlet velocity at the test section inlet. The calming section was made from a stainless-steel tube with an inner diameter of 200 mm and consisted of three components: an inlet mixer (7), the calming section (8) and the square-edged inlet (9). To prevent any possible temperature gradients that could develop as the water flowed from the reservoir to the calming section, the inlet mixer contained stainless-steel shavings that mixed the water. A Pt100 probe was installed in the inlet mixer to measure the bulk inlet water temperature. The square-edged inlet was obtained by connecting the test section (10) flush to the last flange of the calming section. Two bleed valves, one immediately after the inlet mixer and another located before the straws, were used to bleed out entrained air to avoid air bubbles entering the test section.

The test section (10) accommodated two sets of experiments. Firstly, for validation purposes, smooth tube experiments without any twisted tape inserts were conducted and the heat transfer and pressure drop results were compared with literature. The smooth tube had an inner diameter and length of 19 mm and 5.27 m respectively. The second set of experiments was conducted with the CCCTT inserts inside the smooth tube (Fig. 2). The CCCTT inserts had a thickness, δ , of 1 mm, width, W , of 18 mm and a pitch, H , of 90 mm. The details of the manufacturing of the twisted tapes are given in Meyer and Abolarin [57]. For this study, CCCTT inserts consisted of copper plate strips with lengths of 450 mm and a twist ratio, $y = H/W$, of 5. This length ensured five full twists of 180° (or 2.5 twists of 360°) of the tapes. The ends of 12 alternating strips were soldered to each other to form one CCCTT insert. To obtain a total length of 5.27 m, which was the length of the smooth copper test section, the 12th strip had a shorter length of 370 mm. Three

CCCTT inserts were fabricated using different connection angles ($\theta = 0^\circ, 30^\circ$ and 60°). Fig. 3 contains both schematic diagrams and photographs of the CCCTT inserts for connection angles of 0° (Fig. 3(a) and (d)), 30° (Fig. 3(b) and (e)) and 60° (Fig. 3(c) and (f)) respectively.

A pressure transducer (11) was connected to two pressure taps, located at $x = 2.52$ m and $x = 4.97$ m from the inlet of the test section. The distance between the two pressure taps, $L_{\Delta P}$, was thus 2.45 m. Holes with a diameter of 1.6 mm were drilled through the pressure taps and test section using a high-speed drill to prevent burr formations on the inside of the test section. Two differential pressure transducers were used depending on the pressure drops measured. A 0.86 kPa diaphragm was used for the smooth tube experiments, while for the twisted tape inserts, the 0.86 kPa diaphragm was used at lower mass flow rates and a 1.4 kPa diaphragm at higher mass flow rates.

A total of 84 T-type thermocouples (0.25 mm diameter) were used to measure the surface temperatures at 21 measuring stations along the test section (Fig. 2(a)). At each measuring station, four thermocouples (Fig. 2(b)) were soldered at the angles of 0° (top), 90° (left), 180° (bottom) and 270° (right). Care was taken to ensure that the top and bottom thermocouples corresponded to the vertical plane, and the left and right thermocouples corresponded to the horizontal plane. The measuring stations were spaced at 250 mm intervals with the first measuring station located 170 mm from the inlet of the test section ($x/D_i = 9$) and the last measuring station located 5.17 m from the inlet ($x/D_i = 272$). The thermocouples were calibrated within an accuracy of 0.1°C using a thermostat-controlled bath and calibrated Pt100 probes over a temperature range of $17 - 60^\circ\text{C}$. Two constantan heating wires, with a thickness of 0.81 mm each, were tightly coiled around the test section and connected in parallel to the power supply (12) to obtain a constant heat flux boundary condition.

The exit mixer (13) was connected to the exit of the test section. It was fabricated from acetal and had an inner diameter of 19 mm, an outer diameter of 50 mm and a length of 200 mm. Two copper (twisted) mixer plates were placed inside the mixer to ensure that the water exiting the test section was mixed to a uniform temperature. A Pt100 probe installed at the exit mixer was used to measure the bulk exit water temperature. The Pt100 probes installed at the inlet and exit mixers were calibrated to within 0.06°C in a thermostat-controlled bath against a digital thermometer with an accuracy of 0.03°C. After the test section and exit mixer, the water was collected in the reservoir (1) and then pumped to the chiller unit (2) to be cooled.

To minimise heat losses to the surroundings, the inlet mixer, calming section, inlet section, test section and exit mixer were insulated with a flexible, closed-cell, elastomeric nitrile rubber material. The insulation had a low thermal conductivity of 0.037 W/mK and the overall thickness was 144 mm. With this insulation thickness, the heat losses were estimated with one-dimensional heat conduction resistance calculations to be less than 1% of the power input. A computerised data acquisition system (14) was used to record all the mass flow rates, temperatures and pressure drop measurements. The data streamed from this acquisition system was then used for the data reduction.

3. Data reduction

The data reduction methodology followed was in general the same as in refs [57, 65-69]. A linear increase in the mean water temperature within the test section was obtained, because a constant heat flux boundary condition was applied to the test section. The mean water temperatures, $T_m(x)$, at each measuring station, x , on the test section were determined using the measured inlet water temperatures, T_i , measured exit water temperatures, T_e , and the measured heated length, L_h , of the

test section. Eq. (1) therefore allowed for the determination of the water temperature at any position, x , from the inlet where $x = 0$, to the exit where $x = L_e$.

$$T_m(x) = T_i + \left[\frac{T_e - T_i}{L_h} \right] x \quad (1)$$

The properties of water were determined at the measuring stations on the test section as a function of the mean water temperature using the thermophysical correlations of water [70]. The properties were densities, $\rho(x)$, specific heat capacities, $Cp(x)$, thermal conductivities, $k(x)$, dynamic viscosities, $\mu(x)$, and Prandtl numbers, $Pr(x)$. The local values were used for the heat transfer results, while the bulk values (which would be the average between the two pressure taps) were used for the pressure drop results. The bulk water temperatures, T_b , were not calculated at the centre of the tube, but at $x = 3.77$ m (Fig. 2(a)) which is at the centre of the two pressure taps, P_1 and P_2 , where the flow was fully developed. Furthermore, the thermophysical properties of all the bulk variables were determined at the bulk water temperature. The mean surface temperatures, $T_s(x)$, were determined as the average of the four thermocouples (T_{top} , T_{bottom} , T_{left} and T_{right}) at each measuring station on the test section (Fig. 2(b)).

The local Reynolds numbers, $Re(x)$, at each measuring station were determined using the measured mass flow rates, \dot{m} , of the water that flowed through the test section, the measured inner diameter of the test section, D_i , the local dynamic viscosities, $\mu(x)$, at each measuring station, and the cross-sectional area, $A_c = \pi D_i^2/4$, of the test section:

$$Re(x) = \frac{\dot{m} D_i}{A_c \mu(x)} \quad (2)$$

Everts and Meyer [66] defined the width of the transitional flow regime, ΔRe , as the difference between the Reynolds numbers at which transition started, Re_{cr} , and ended, Re_{qt} :

$$\Delta Re = Re_{qt} - Re_{cr} \quad (3)$$

The heat transfer rates to the water, \dot{Q} , were determined from the measured mass flow rates, \dot{m} , the differences in measured temperatures between the exit, T_e , and inlet, T_i , of the test section and the bulk specific heat capacities, Cp_b , as:

$$\dot{Q} = \dot{m}Cp_b[T_e - T_i] \quad (4)$$

It should be noted that the bulk specific heat capacity in Eq. (4) was calculated at the centre of the tube.

The electrical power supplied, \dot{Q}_e , to the heating wires was determined using the sum of the product of the currents, I_1 and I_2 , through each heating wire and the voltage drops across each heating wire, ΔV_1 and ΔV_2 , as:

$$\dot{Q}_e = I_1\Delta V_1 + I_2\Delta V_2 \quad (5)$$

The heat transfer rates to the water, \dot{Q} , were regularly monitored and compared with that of the electrical power supplied, \dot{Q}_e , by calculating the energy balance error, eb , as:

$$eb = \left| 1 - \frac{\dot{Q}}{\dot{Q}_e} \right| \times 100 \quad (6)$$

The heat fluxes, \dot{q} , were determined as follows:

$$\dot{q} = \frac{\dot{Q}}{A_s} \quad (7)$$

where the inner surface area, A_s , was determined from the measured inner diameter, D_i and measured heated length, L_h , as $A_s = \pi D_i L_h$. The heat fluxes, \dot{q} , were determined using the heat transfer rates to the water, \dot{Q} , as this was considered to be more accurate. The reason is that the electrical power supplied, \dot{Q}_e , to the test section was slightly higher than the heat transfer rate to the water, \dot{Q} , due to small heat losses that occurred from the heated test section to the environment.

The heat transfer coefficients, $h(x)$, at each measuring station were determined from the heat fluxes, \dot{q} , the mean surface temperatures, $T_s(x)$, and the mean water temperatures, $T_m(x)$, as:

$$h(x) = \frac{\dot{q}}{[T_s(x) - T_m(x)]} \quad (8)$$

The Nusselt numbers, $Nu(x)$, at each measuring station were determined as:

$$Nu(x) = \frac{h(x)D_i}{k(x)} \quad (9)$$

The Colburn j -factors, $j(x)$, at each measuring station were determined as:

$$j(x) = \frac{Nu(x)}{[Pr(x)]^{1/3} Re(x)} \quad (10)$$

The modified Grashof numbers, $Gr^*(x)$, which is a function of heat flux instead of temperature difference, at each measuring station were determined as:

$$Gr^*(x) = \frac{g\dot{q}\beta(x)D_i^4}{k(x)[\nu(x)]^2} \quad (11)$$

where, the gravitational acceleration, g , was taken as 9.81 m/s^2 , and the kinematic viscosities, $\nu(x)$, were determined as the ratio of densities, $\rho(x)$, to dynamic viscosities, $\mu(x)$.

The friction factors, f , across the measured pressure drop length, $L_{\Delta P}$, between the two pressure taps, were determined as:

$$f = \frac{\Delta P \rho_b D_i^5 \pi^2}{8 \dot{m}^2 L_{\Delta P}} \quad (12)$$

Similar to the local parameters, the bulk Reynolds numbers and bulk modified Grashof numbers, between the two pressure taps, were calculated using the bulk fluid properties in Eqs. (2) and (11).

4. Experimental procedure and test matrix

Experiments were conducted at 60 different mass flow rates to cover the transitional flow regime as well as sufficient parts of the laminar and turbulent flow regimes. CCCTT insert with three different connection angles ($\theta = 0^\circ, 30^\circ$ and 60°) were tested at four different heat fluxes of 1.35, 2, 3 and 4 kW/m². This resulted in a total of 720 mass flow rates for the different combinations of connection angles and heat fluxes.

After start-up, approximately three hours were permitted for the system to reach the initial steady-state conditions. A steady-state condition was assumed once the standard deviations of the measured mass flow rates, temperatures and pressures drops were constant for a period of 10 - 15 minutes. Once steady-state conditions were reached, a total of 400 data points of the temperatures (inlet water temperatures, surface temperatures on the test section and exit water temperatures), mass flow rates and pressure drops were logged and the currents and the voltage drops were recorded. The average of the 400 data points was regarded as one measurement.

After a set of data was logged, the mass flow rate was decreased by approximately 1.7% to the next Reynolds number. As the changes in the mass flow rates were small, steady-state conditions between the Reynolds number decrements were obtained much faster than the initial steady state. Approximately 10 – 15 minutes was required in the turbulent flow regime, 20 - 35 minutes was required in the transitional flow regime, while 15 - 20 minutes was required in the laminar flow regime. The energy balance errors (Eq. 6) during the experiments were continuously monitored and varied from one flow regime to another. The energy balance error ranges were 3 – 5%, 2 – 3% and 2 – 4% in the laminar, transitional and turbulent flow regimes respectively. The maximum error balance errors were found in the laminar flow regime where maximum surface temperatures were obtained due to the small mass flow rates.

5. Uncertainty analysis

The uncertainties were calculated as prescribed by Dunn [71] using a 95% confidence level. The manufacturer specified accuracies (Table 1) were used to calculate the bias errors, while the precision errors were determined from the standard deviation of the 400 data points taken at each mass flow rate. Fig. 4 compares the local Reynolds number uncertainties (Fig. 4(a)), local Colburn j -factor uncertainties (Fig. 4(b)) and friction factor uncertainties (Fig. 4(c)) of the CCCTT insert, CTT insert at a twist ratio of 5 and a smooth tube, all at a heat flux of 4 kW/m². This comparison is done to explain the differences in the uncertainties especially in the transitional flow regime. The uncertainties were plotted as a function of local Reynolds number, $Re(x)$, in Figs. 4(a) and 4(b), but as a function of bulk Reynolds number in Fig. 4(c). The reason being that the heat transfer values were local values while the friction factor values were the averages between the two pressure taps in Fig. 2(a). Fig. 4 also identifies the data in the different flow regimes, as described in Meyer and Abolarin [57]. The laminar data (“ L ”-values) is always to the left of the transition (“ ΔRe ”-values), while the turbulent data would then be to the right of the transition data.

Fig. 4(a) shows that the Reynolds number uncertainties decreased as the mass flow rates (which were directly proportional to the Reynolds number) increased. The discontinuity between points “ A ” and “ B ” occurred because different Coriolis mass flow meters were used for the low and high mass flow rate experiments. From point “ B ”, a Coriolis mass flow meter with a higher range was used. However, all the uncertainties were low and varied between a maximum of 1.6% and a minimum of 1%.

In the laminar flow regime, the Colburn j -factor uncertainties (Fig. 4(b)) of the smooth tube were less than 4%; however, it increased to 31% in the transitional flow regime. The significant increase was due to the increase in standard deviation of the 400 temperature measuring points compared

with the laminar and turbulent flow regimes. For the CCCTT and CTT inserts, the laminar and transitional uncertainties varied between 7.8% and 5.4%. The uncertainties of the two twisted tape inserts in the transitional flow regimes were thus much lower than for a smooth tube, because the inserts dampened the large fluctuations that are usually associated with the transitional flow regime [66]. A general trend in the turbulent flow regime was that the uncertainties increased with increasing Reynolds number. This was as expected because the temperature differences between the wall and fluid decreased with increasing Reynolds numbers for constant heat flux applications. However, all the uncertainties were less than 13% for the CCCTT inserts, and specifically in the transitional flow regime, which was the focus of this study, it was less than 7%.

Fig. 4(c) compares the friction factor uncertainties of the CCCTT insert, CTT insert and smooth tube. In all the flow regimes, the friction factor uncertainties decreased with increasing Reynolds number. Because the mass flow rate meter was located upstream of the test section, the increased friction factor uncertainties in the transitional flow regime, due to the mass flow rate fluctuations in the smooth tube, were not visible. However, these fluctuations have been confirmed by Everts and Meyer [66] who had a mass flow rate meter downstream of the test section. Furthermore, at any Reynolds number, the smooth tube had the highest uncertainty as its pressure drops were much lower than that of the tubes with the tape inserts. In the laminar flow regime, the maximum friction factor uncertainty was 23% in the smooth tube, while it was approximately 18% for the CTT and CCCTT inserts. In the transitional flow regime, the maximum uncertainties varied between 4.5% and 6.5% for all three tubes. In the turbulent flow regime, the uncertainties for all three tubes were less than 5%.

6. Validation with literature

The Colburn j -factor and friction factor results in the smooth tube (without a twisted tape insert) were compared with well-known and relevant smooth tube correlations in literature. The validation results have been described in detail by Meyer and Abolarin [57]. In general, the results showed that the laminar Colburn j -factors compared well with the correlation of Morcos and Bergles [72] with an average deviation of 7%. In the turbulent flow regime, the Colburn j -factors correlated well with the correlation of Ghajar and Tam [59] with a maximum deviation of less than 5%.

The laminar friction factors were compared with the correlations of Tam and Ghajar [62] and Test [73] and had a maximum deviation of less than 5%. In the turbulent flow regime, the friction factors were compared with the correlations of Blasius [74] and Allen and Eckert [75] and the deviations were approximately 4%.

Furthermore, the turbulent Colburn j -factors and friction factors of the CCCTT inserts were compared with the correlations of Eiamsa-ard and Promvong [4] and the deviations were within 5% and 15% respectively. Although the deviation of the friction factors were significantly higher than for the Colburn j -factors, it was still within the accuracy of the correlation, because the correlation of Eiamsa-ard and Promvong [4] was within 15% deviation from their experimental data. This indicated that the experimental results in this study excellently agreed with literature and as such the results presented in the Section 7 can be relied upon.

7. Results and discussion

For forced convection laminar flow (at a Reynolds number of 1 000 in a smooth tube) the flow was expected to be fully developed at $x/D_i = 0.12RePr = 840$ [69] and for turbulent flow at $x/D_i \approx 10$. Although the test section considered was not a smooth tube this should at least give an

order of magnitude estimate. However, similar to the results obtained by Meyer and Abolarin [57], the local Nusselt numbers indicated that in all three flow regimes (laminar, transitional and turbulent) the flow was developing at the first measuring station, $x/D_i = 9$, and fully developed for $x/D_i \geq 22$ when CCCTT inserts were used. The significant decrease in the laminar thermal entrance length was due to the fluid rotation caused by the tape inserts as well as free convection effects that led to mixed convection [69]. The heat transfer results could thus be presented in two ways: either as the average between $x/D_i = 22$ and $x/D_i = 272$, or at a specific measuring station as was used in the work of Ghajar and Tam [59, 60, 76]. Similar to Ghajar and Tam [59, 60, 76] and Meyer and Abolarin [57], the results were presented at a specific measuring station, $x/D_i = 246$. Furthermore, due to the direct relationship between heat transfer and pressure drop that exists in all flow regimes, the heat transfer results were investigated in terms of the Colburn j -factors [68].

The transitional flow regime, which was the main focus of this study, was identified using the linear line method prescribed by Meyer and Abolarin [57]. As illustrated in Fig. 5, for a CCCTT insert with a twist ratio of $y = 5$, connection angle of $\theta = 60^\circ$, and heat flux of 1.35 kW/m^2 , this method involved linear fits (on a log-log scale) of the data in the laminar, transitional and turbulent flow regimes when the Colburn j -factors or friction factors were plotted as a function of Reynolds number. The laminar flow regime was identified by the “ $L-L$ ” line which excluded the data points close to the critical Reynolds number. The transitional flow regime was marked by the “ $R-R$ ” line and the data points near the start and the end of the transitional flow regime were excluded in the fitting of this line. The turbulent flow regime was identified by the “ $T-T$ ” line. The intersection of the laminar “ $L-L$ ” and transitional “ $R-R$ ” curve fits indicated that transition started at a Reynolds number of 529. Also, the intersection of the transitional “ $R-R$ ” and turbulent “ $T-T$ ” curve fits, indicated that the transitional flow regime ended at a Reynolds number of 847.

7.1 Comparison of the CCCTT insert with PUCTT and CTT inserts

Fig. 6 compares the Colburn j -factors (Fig. 6(a)) and friction factors (Fig. 6(b)) as a function of Reynolds number of the CCCTT insert (changing the flow direction every 450 mm) at a connection angle of 60° , with a PUCTT22 insert (peripheral u-cuts) [77] with a depth ratio of 0.216 and CTT insert that rotated the flow in only one direction. All the twisted tape inserts had a twist ratio of $y = 5$ and the experiments were conducted at a heat flux of 2 kW/m^2 . It should be noted that for the Colburn j -factors, the lowest uncertainties occurred in the laminar flow regime where temperature differences were high, while the lowest friction factor uncertainties were found in the turbulent flow regime where pressure drops were higher. Therefore, in the laminar flow regime the Colburn j -factor data is more accurate while the friction factor data is more accurate in the turbulent flow regime. In cases where small differences occurred between the CCCTT, PUCTT22 and CTT inserts in the laminar flow regime (as in some cases in this paper); the Colburn j -factor data are more representative of the real differences. For cases with small differences in the turbulent flow regime, the friction factors are more representative of the real differences. This has been shown by the heat transfer and pressure drop analogy work of Everts and Meyer [68].

Similar to the results reported in literature [40-42, 45, 46, 78, 79], the Colburn j -factors (Fig. 6(a)) indicate that there were very small differences in the results of the three twisted tapes in the laminar flow regime. Therefore, changing the flow rotation direction or modifying the twisted tape inserts were not effective heat transfer techniques in the laminar flow regime. In the turbulent flow regime, the heat transfer enhancement varied between approximately 4% and 15%.

Significant heat transfer enhancement was also obtained in the transitional flow regime. At a Reynolds number of 1 000, the Colburn j -factors of the CCCTT insert were approximately 30% and 46% higher than those of the PUCTT22 insert and CTT insert respectively. Furthermore, the transitional flow regime occurred significantly earlier (at lower Reynolds numbers) when a CCCTT insert was used. The transitional flow regime started, Re_{cr} , and ended, Re_{qt} , at Reynolds

numbers of 1 023 and 1 604 for the CTT insert, at 796 and 1 344 for the PUCTT22 insert and at 685 and 978 for the CCCTT insert. Similar results were obtained in the friction factor data in Fig. 6(b). This can be expected as Everts and Meyer [68], determined that the Colburn analogy is also valid in the transitional flow regime and that the start and end of transitional flow regime will always occur at the same mass flow rate for heat transfer and pressure drop data. For the results in this study (with heat transfer results as a function of local Reynolds numbers and friction factors as a function of bulk Reynolds number), the Reynolds numbers for the start and end of transition were not exactly the same. This is due to the different temperatures at which the fluid properties, mainly the viscosities, were calculated.

No significant difference was found in the laminar friction factor data in Fig. 6(b). In the transitional flow regime, it was found that at a Reynolds number of 1 000, the friction factors of the CCCTT insert were approximately 24% higher than that of the CTT insert and 18% lower than that of the PUCTT insert. Similar to the Colburn j -factors, the transitional flow regime started and ended first for the CCCTT insert. For the CTT insert the start and end of transition were at Reynolds numbers of 923 and 1 504, while 747 and 1298 for the PUCTT22 insert and for the CCCTT insert they were at 637 and 932 respectively.

In the turbulent flow regime, the friction factors of the CCCTT insert were slightly higher than for the CTT insert and significantly lower than the PUCTT22 insert. For instance, at Reynolds numbers of 1 540 and 5 897, the friction factors of the CCCTT insert were 12% and 7% respectively higher than those of the CTT insert, while they were 22% and 58% respectively lower than those of the PUCTT22 insert. Because the CCCTT insert caused the flow path to change rotation direction (from clockwise to counter clockwise) 12 times, the flow was continually disturbed and the flow path length was increased. This led to the slight increase in friction factors

compared with the CTT insert. The discontinuity at “C” in the Fig. 6(b) occurred because different pressure transducer diaphragms were used due to the range limitations.

It can therefore be concluded that no enhancement occurred in the laminar and turbulent flow regimes with a CCCTT insert compared with PUCTT and CTT inserts. However, significant heat transfer enhancements were observed in the transitional flow regime and transition occurred earlier when CCCTT inserts were used.

7.2 Connection angle

Fig. 7 compares the Colburn j -factors (Fig. 7(a)) and friction factors (Fig. 7(b)) as a function of Reynolds number for different connection angles ($\theta = 0^\circ, 30^\circ$ and 60°) at a heat flux of 3 kW/m^2 . Fig. 7(a) indicates that using different connection angles led to no heat transfer enhancement in the laminar flow regime. In the turbulent flow regime at a Reynolds number of 2 000, an increase of 13% and 23% compared to a connection angle of 0° , occurred for connection angles of 30° and 60° respectively. Similar enhancement trends occurred in the turbulent flow regime for the friction factors in Fig. 7(b). Therefore, the increased disturbance caused by the connection angle enhanced mixing inside the test section which led to increased heat transfer coefficients. However, this enhancement decreased with increasing Reynolds numbers, because the effect of the disturbance caused by the connection became less significant compared with the turbulent inertia of the fluid.

For the Colburn j -factors (Fig. 7(a)), the transition started and ended at Reynolds numbers of 997 and 1 308, 973 and 1 271, and 920 and 1 200 for the respective connection angles of $0^\circ, 30^\circ$ and 60° . The transitional flow regime was thus occurred earlier as the connection angle increased. At a Reynolds number of 1 000, the Colburn j -factors were 0.0175, 0.0190 and 0.0219 respectively, for connection angles of $0^\circ, 30^\circ$ and 60° . Thus, the Colburn j -factors also increased with

connection angles and were 25% higher for a connection angle of 60° than for a connection angle of 0° . The Reynolds numbers at which the transitional flow regime started, Re_{cr} , ended, Re_{qt} , as well as the width of the transitional flow regime, ΔRe [66], are summarised in Table 3. It should be noted that the Colburn j -factor results and friction factor results were very similar and the same conclusions can be made from both.

Table 3 indicates that, for all heat fluxes, the critical Reynolds number decreased with increasing connection angle. This was due to the increased disturbance and swirl caused by the connection angle, combined with the sudden change in flow direction, that disturbed the boundary layer. Table 3 also indicates that similar to the start of the transitional flow regime, the end of the transitional flow regime, Re_{qt} , occurred earlier with increasing connection angle. Furthermore, as the connection angle was increased from 0° to 60° the width of the transitional flow regime, ΔRe , decreased from a Reynolds number range of 311 to 280.

It can therefore be concluded that an increase in connection angle caused a greater disturbance inside the test section that not only enhanced the heat transfer in the transitional flow regime, but also caused transition to occur earlier and the width of the transitional flow regime to decrease. However, there were no significant enhancements in the laminar and turbulent flow regimes.

7.3 Heat flux

Fig. 8 compares the Colburn j -factors (Fig. 8(a)) and friction factors (Fig. 8(b)) as a function of Reynolds number at different heat fluxes for a CCCTT insert with a connection angle of $\theta = 30^\circ$. This figure indicates that the increasing free convection effects due to the increased heat flux caused the Colburn j -factors and friction factors in the laminar flow regime to increase [41, 44, 66, 68]. At a laminar Reynolds number of 500, the Colburn j -factor enhancement was 103% when the

heat flux was increased from 1.35 kW/m^2 to 2 kW/m^2 . As expected, the heat flux did not affect the results in the turbulent flow regime, because free convection effects were negligible compared with the inertia forces[66].

The Colburn j -factors in Fig. 8(a) also indicate that the start, end and width of the transitional flow regime were significantly affected by free convection effects. At a heat flux of 1.35 kW/m^2 , the transitional flow regime started and ended at Reynolds numbers of 563 and 894, respectively. As the heat flux was increased to 4 kW/m^2 , both the start and end of transition were delayed to Reynolds numbers of 1 184 and 1 465, respectively. Furthermore, the width of the transitional flow regime, ΔRe , decreased from a Reynolds number range of 331 at a heat flux of 1.35 kW/m^2 , to 281 at a heat flux of 4 kW/m^2 . The same trends were found in the friction factor results (Fig. 8(b) and Table 3), the results of the other connection angles, as well as previous studies [57, 59, 65-69]. Everts and Meyer [66] explained that although free convection effects caused the transitional flow regime to occur at lower mass flow rates, the Reynolds numbers at which transition started and ended increased. The gradient of the fluid temperature along the test section increased with increasing heat flux, which led to decreasing viscosities and increased Reynolds numbers. Furthermore, Everts and Meyer [65, 66, 68] also found that as free convection effects were increased, a shorter tube length was required for the flow to transition from laminar to turbulent along the tube length, which explains why the width of the transitional flow regime decreased with increasing heat flux.

In general, it can therefore be concluded that an increase in heat flux significantly enhanced the heat transfer in the laminar flow regime, delayed transition and decreased the width of the transitional flow regime. However, an increase in heat flux had no significant effect in the turbulent flow regime.

7.4 Correlations

Three sets of correlations were developed to predict the experimental data of this study: (1) Correlations to predict the start and the end of the transitional flow regime as a function of connection angle (Fig. 9). (2) Correlations to predict the Colburn j -factors in the laminar, transitional and turbulent flow regimes (Fig. 10). (3) Correlations to predict the friction factors in the same three flow regimes. The ranges and performance of the different correlations are summarised in Table 4. In Fig. 9, the filled markers represent the Colburn j -factor data, while the empty markers represent the corresponding friction factor data. In Fig. 10, the filled black markers represent the data at a heat flux of 1.35 kW/m^2 , while the empty red, blue and magenta markers represent the results at heat fluxes of 2 kW/m^2 , 3 kW/m^2 and 4 kW/m^2 respectively. Furthermore, the squares, circles and triangles represent the connection angles of 0° , 30° and 60° .

7.4.1 Start and end of the transitional flow regime

Figs. 7 and 8 indicated that the start and the end of the transitional flow regime were influenced by connection angle, θ , and free convection effects (heat flux). To account for different connection angles, a $\cos\theta$ -term was introduced, while the modified Grashof number, Gr^* , was used to account for free convection effects. The critical Reynolds numbers, Re_{cr} , in Table 3 were divided by $[Gr^*(x)]^{0.416}$ and $\cos\theta$ in Fig. 9(a). The exponent 0.416 was found through trial and error. A power curve fit was done through the data points to obtain the following correlation to predict the start of the transitional flow regime:

$$Re_{cr}(x) = 1.46[Gr^*(x)]^{0.416}[\cos\theta]^{0.158} \quad (13)$$

A similar approach was followed to determine the end of the transitional flow regime from the results in Fig. 9(b):

$$Re_{qt}(x) = 19.4[Gr^*(x)]^{0.275}[\cos\theta]^{0.143} \quad (14)$$

The corresponding bulk Reynolds numbers for the start, Re_{crb} , and end, Re_{qtb} , of the transitional flow regime in terms of the friction factors were obtained by replacing the $Gr^*(x)$ in Eqs. (13) and (14) with the bulk modified Grashof number, Gr_b^* . The ranges and performance of Eqs. (13) and (14) are summarised in Table 4. This table indicates that the start and end of transitional flow regime of both the Colburn j -factor and friction factor results could be determined within 6%.

7.4.2 Colburn j -factors

The laminar Colburn j -factors decreased with increasing Reynolds number (Fig. 5) and increased with increasing free convection effects (Fig. 8(a)), but were not significantly affected by the connection angle (Fig. 7(a)). Therefore, the laminar Colburn j -factors were divided by $[Gr^*(x)]^{0.61}$ to account for free convection effects and the results were plotted as a function of Reynolds number in Fig. 10(a). Again, the power of 0.61 was determined through trial and error. The following laminar Colburn j -factor correlation was obtained through a power curve fit:

$$j_L(x) = 6.52[Re(x)]^{-2.25}[Gr^*(x)]^{0.61} \quad (15)$$

Table 4 indicates that the average and maximum deviations were 3 and 12% respectively.

In the transitional flow regime, it was found that the Colburn j -factors were significantly influenced by the Reynolds number (Fig. 5), connection angle (Fig. 7(a)), as well as the free convection effects (Fig. 8(a)). Therefore, the following correlation was developed to predict the Colburn j -factors in the transitional flow regime:

$$j_R(x) = 2.37[Re(x)]^{-0.337}[Gr^*(x)]^{-0.168}[\cos\theta]^{-0.356} \quad (16)$$

Table 4 indicates that Eq. (16) was able to predict all the Colburn j -factors in the transitional flow regime with an average deviation of 3% and a maximum deviation of 13%.

Figs. 7(a) and 8(a) indicated that the turbulent Colburn j -factors were a function of Reynolds number and connection angle, but not a function of modified Grashof number because free convection effects were suppressed by the inertia forces of the fluid [66]. The turbulent Colburn j -factor correlation was developed from the results in Fig. 10(c):

$$j_T(x) = 1.57[Re(x)]^{-0.641}[\cos\theta]^{-0.102} \quad (17)$$

Eq. (17) performed very well and was able to predict the experimental data with average deviation of 2% and a maximum deviation of 13%.

7.4.3 Friction factors

Similarly, the following correlations were developed to predict the friction factors in the laminar, transitional and turbulent flow regimes (friction factor figures corresponding to Fig. 10 were not included in this paper as it looks similar):

$$f_L = 10.6[Re_b]^{-0.849}[Gr_b^*]^{0.141}[\cos\theta]^{-0.176} \quad (18)$$

$$f_R = 5.77[Re_b]^{-0.252}[Gr_b^*]^{-0.0815}[\cos\theta]^{-0.214} \quad (19)$$

$$f_T = 11.6[Re_b]^{-0.517}[\cos\theta]^{-0.079} \quad (20)$$

The ranges and performance of Eqs. (18) – (20) are summarised in Table 4. This table indicates all the correlations performed well and were able to predict the friction factors in the laminar, transitional and turbulent flow regimes with average deviations of 5%, 2% and 1% respectively.

8. Conclusions

The heat transfer and pressure drop characteristics of a smooth horizontal tube with CCCTT inserts at different connection angles were experimentally investigated in the laminar, transitional and turbulent flow regimes for different constant heat fluxes. The CCCTT inserts consisted of clockwise and counter clockwise segments with a twist ratio of 5 and length of 450 mm. Therefore, flow rotation was changed every 450 mm and the different segments were connected at connection angles of 0° , 30° and 60° . Experiments were conducted at four different constant heat fluxes and a total of 720 experimental data points was obtained in this study.

The comparison of the Colburn j -factor and friction factor results of the CCCTT insert with the CTT and PUCTT inserts showed no enhancement in the laminar flow regime. In the transitional flow regime significant heat transfer enhancements occurred and transition of the CCCTT occurred earlier than with the PUCTT and CTT inserts. In the turbulent flow regime, the heat transfer enhancements of the CCCTT insert were slightly better than that of the CTT insert.

When different connection angles were compared it was found that the increased disturbance created by an increased connection angle enhanced mixing inside the test section, which led to increased heat transfer. Furthermore, it also caused transition to occur at lower Reynolds numbers. However, the connection angle had no significant effect in the laminar and turbulent flow regimes. An increase in heat flux was found to enhance heat transfer in the laminar flow regime and delay transition, however, the turbulent flow regime remained unaffected.

Correlations to predict the start and end of the transitional flow regime, as well as the Colburn j -factors and friction factors in the laminar, transitional, and turbulent flow regimes, were developed. These correlations were developed as a function of the Reynolds number, connection angle, and

modified Grashof number, to account for different connection angles as well as free convection effects where relevant.

Acknowledgement

The authors appreciate the sponsorships received in South Africa from the following institutions and organisations throughout the period of the experimentation: The Department of Science and Technology (DST), National Research Foundation (NRF), and University of Pretoria. The first author was a PhD student that was supervised by the second author (post-doctoral fellow) and the third author (professor).

References

- [1] M. Pan, I. Bulatov, R. Smith, Novel MILP-based optimization method for retrofitting heat exchanger networks, *Computer Aided Chemical Engineering*, 30 (2012) 567-571.
- [2] P.S. Bandyopadhyay, U.N. Gaitonde, S.P. Sukhatme, Influence of free convection on heat transfer during laminar flow in tubes with twisted tapes, *Experimental Thermal and Fluid Science*, 4(5) (1991) 577-586.
- [3] H. Safikhani, F. Abbasi, Numerical study of nanofluid flow in flat tubes fitted with multiple twisted tapes, *Advanced Powder Technology*, 26(6) (2015) 1609-1617.
- [4] S. Eiamsa-ard, P. Promvonge, Performance assessment in a heat exchanger tube with alternate clockwise and counter-clockwise twisted-tape inserts, *International Journal of Heat and Mass Transfer*, 53(7-8) (2010) 1364-1372.
- [5] S.W. Hong, A.E. Bergles, Augmentation of laminar flow heat transfer in tubes by means of twisted-tape inserts, *Journal of Heat Transfer*, 98(2) (1976) 251-256.

- [6] S.W. Chang, J.Y. Gao, H.L. Shih, Thermal performances of turbulent tubular flows enhanced by ribbed and grooved wire coils, *International Journal of Heat and Mass Transfer*, 90 (2015) 1109-1124.
- [7] R.K. Ali, M.A. Sharafeldein, N.S. Berbish, M.A. Moawed, Convective heat transfer enhancement inside tubes using inserted helical coils, *Thermal Engineering*, 63(1) (2016) 42-50.
- [8] A. Garcia, J.P. Solano, P.G. Vicente, A. Viedma, Enhancement of laminar and transitional flow heat transfer in tubes by means of wire coil inserts, *International Journal of Heat and Mass Transfer*, 50(15-16) (2007) 3176-3189.
- [9] A. García, J.P. Solano, P.G. Vicente, A. Viedma, The influence of artificial roughness shape on heat transfer enhancement: corrugated tubes, dimpled tubes and wire coils, *Applied Thermal Engineering*, 35 (2012) 196-201.
- [10] A. Nouri-Borujerdi, M.E. Nakhchi, Heat transfer enhancement in annular flow with outer grooved cylinder and rotating inner cylinder: Review and experiments, *Applied Thermal Engineering*, 120 (2017) 257-268.
- [11] A. Nouri-Borujerdi, M.E. Nakhchi, Optimization of the heat transfer coefficient and pressure drop of Taylor-Couette-Poiseuille flows between an inner rotating cylinder and an outer grooved stationary cylinder, *International Journal of Heat and Mass Transfer*, 108 (2017) 1449-1459.
- [12] S.S. Chougule, S.K. Sahu, Heat transfer and friction characteristics of Al₂O₃/water and CNT/water nanofluids in transition flow using helical screw tape inserts – a comparative study, *Chemical Engineering and Processing: Process Intensification*, 88 (2015) 78-88.
- [13] N. Moghadas Zade, S. Akar, S. Rashidi, J. Abolfazli Esfahani, Thermo-hydraulic analysis for a novel eccentric helical screw tape insert in a three dimensional tube, *Applied Thermal Engineering*, 124 (2017) 413-421.

- [14] S. Rashidi, N.M. Zade, J.A. Esfahani, Thermo-fluid performance and entropy generation analysis for a new eccentric helical screw tape insert in a 3D tube, *Chemical Engineering and Processing: Process Intensification*, 117 (2017) 27-37.
- [15] K. Wongcharee, S. Eiamsa-ard, Friction and heat transfer characteristics of laminar swirl flow through the round tubes inserted with alternate clockwise and counter-clockwise twisted-tapes, *International Communications in Heat and Mass Transfer*, 38(3) (2011) 348-352.
- [16] A. Boonloi, W. Jedsadaratanachai, Turbulent forced convection and heat transfer characteristic in a circular tube with modified-twisted tapes, *Journal of Thermodynamics*, 2016 (2016) 1-16.
- [17] S.W. Chang, B.J. Huang, Thermal performances of tubular flows enhanced by ribbed spiky twist tapes with and without edge notches, *International Journal of Heat and Mass Transfer*, 73 (2014) 645-663.
- [18] W. Changcharoen, P. Somravysin, S. Eiamsa-ard, Thermal and fluid flow characteristics in a tube equipped with peripherally-cut dual twisted tapes, *Open Engineering*, 5(1) (2015) 89-98.
- [19] S. Chokphoemphun, C. Hinthao, S. Eiamsa-ard, P. Promvonge, C. Thianpong, Thermal performance in circular tube with co/counter-twisted tapes, in: *Advanced Materials Research*, 2014, pp. 1198-1202.
- [20] S. Chokphoemphun, M. Pimsarn, C. Thianpong, P. Promvonge, Thermal performance of tubular heat exchanger with multiple twisted-tape inserts, *Chinese Journal of Chemical Engineering*, 23(5) (2015) 755-762.
- [21] S. Eiamsa-ard, K. Kiatkittipong, W. Jedsadaratanachai, Heat transfer enhancement of TiO₂/water nanofluid in a heat exchanger tube equipped with overlapped dual twisted-tapes, *Engineering Science and Technology, an International Journal*, 18(3) (2015) 336-350.

- [22] S. Eiamsa-ard, K. Nanan, K. Wongcharee, K. Yongsiri, C. Thianpong, Thermohydraulic performance of heat exchanger tube equipped with single-, double-, and triple-helical twisted tapes, *Chemical Engineering Communications*, 202(5) (2015) 606-615.
- [23] N. Piriyarungrod, M. Kumar, C. Thianpong, M. Pimsarn, V. Chuwattanakul, S. Eiamsa-ard, Intensification of thermo-hydraulic performance in heat exchanger tube inserted with multiple twisted-tapes, *Applied Thermal Engineering*, 136 (2018) 516-530.
- [24] S. Eiamsa-ard, C. Thianpong, P. Eiamsa-ard, P. Promvong, Convective heat transfer in a circular tube with short-length twisted tape insert, *International Communications in Heat and Mass Transfer*, 36(4) (2009) 365-371.
- [25] I. Zeynali Famileh, J. Abolfazli Esfahani, Experimental investigation of wet flue gas condensation using twisted tape insert, *International Journal of Heat and Mass Transfer*, 108 (2017) 1466-1480.
- [26] S.W. Chang, W.L. Cai, R.S. Syu, Heat transfer and pressure drop measurements for tubes fitted with twin and four twisted fins on rod, *Experimental Thermal and Fluid Science*, 74 (2016) 220-234.
- [27] P.V. Durga Prasad, A.V.S.S.K.S. Gupta, Experimental investigation on enhancement of heat transfer using Al_2O_3 /water nanofluid in a u-tube with twisted tape inserts, *International Communications in Heat and Mass Transfer*, 75 (2016) 154-161.
- [28] Z.H. Ayub, S.F. Al-Fahed, The effect of gap width between horizontal tube and twisted tape on the pressure drop in turbulent water flow, *International Journal of Heat and Fluid Flow*, 14(1) (1993) 64-67.
- [29] M.M.K. Bhuiya, A.K. Azad, M.S.U. Chowdhury, M. Saha, Heat transfer augmentation in a circular tube with perforated double counter twisted tape inserts, *International Communications in Heat and Mass Transfer*, 74 (2016) 18-26.

- [30] C. Chang, C. Xu, Z.Y. Wu, X. Li, Q.Q. Zhang, Z.F. Wang, Heat transfer enhancement and performance of solar thermal absorber tubes with circumferentially non-uniform heat flux, in: *Energy Procedia*, 2015, pp. 320-327.
- [31] S. Al-Fahed, L. Chamra, W. Chakroun, Pressure drop and heat transfer comparison for both microfin tube and twisted-tape inserts in laminar flow, *Experimental Thermal Fluid Science*, 18(4) (1998) 323-333.
- [32] S.W. Chang, K.W. Yu, M.H. Lu, Heat transfer in tubes fitted with single, twin and tripple twisted tapes, *Journal of Experimental Heat Transfer*, 18 (2005) 279-294.
- [33] M.K. Abdolbaqi, W.H. Azmi, R. Mamat, N.M.Z.N. Mohamed, G. Najafi, Experimental investigation of turbulent heat transfer by counter and co-swirling flow in a flat tube fitted with twin twisted tapes, *International Communications in Heat and Mass Transfer*, 75 (2016) 295-302.
- [34] M.M.K. Bhuiya, M.S.U. Chowdhury, M. Saha, M.T. Islam, Heat transfer and friction factor characteristics in turbulent flow through a tube fitted with perforated twisted tape inserts, *International Communications in Heat and Mass Transfer*, 46 (2013) 49-57.
- [35] G.J. Kidd, Heat transfer and pressure drop for nitrogen flowing in tubes containing twisted tapes, *AIChE Journal*, 15(4) (1969) 581-585.
- [36] O. Klepper, Heat Transfer Performance of Short Twisted Tapes, National Lab, Tennessee., Oak Ridge, 1972.
- [37] S.K. Saha, A. Dutta, Thermohydraulic study of laminar swirl flow through a circular tube fitted with twisted tapes, *Journal of Heat Transfer*, 123(3) (2001) 417-427.
- [38] S.K. Saha, S. Bhattacharyya, P.K. Pal, Thermohydraulics of laminar flow of viscous oil through a circular tube having integral axial rib roughness and fitted with center-cleared twisted-tape, *Experimental Thermal and Fluid Science*, 41 (2012) 121-129.

- [39] S. Bhattacharyya, S.K. Saha, Thermohydraulics of laminar flow through a circular tube having integral helical rib roughness and fitted with centre-cleared twisted-tape, *Experimental Thermal and Fluid Science*, 42 (2012) 154-162.
- [40] F. Bishara, M.A. Jog, R.M. Manglik, Heat transfer and pressure drop of periodically fully developed swirling laminar flows in twisted tubes with elliptical cross sections, *ASME International Mechanical Engineering Congress and Exposition, Heat Transfer, Fluid Flows, and Thermal Systems, Parts A, B and C*, 9 (2009) 1131-1137.
- [41] R.M. Manglik, A.E. Bergles, Heat transfer and pressure drop correlations for twisted-tape inserts in isothermal tubes: Part I—laminar flows, *Journal of Heat Transfer*, 115(4) (1993) 881-889.
- [42] J.P. Du Plessis, D.G. Kroger, Friction factor prediction for fully developed laminar twisted-tape flow, *International Journal of Heat and Mass Transfer*, 27(1) (1984) 2095-2100.
- [43] J.P. Du Plessis, D.G. Kröger, Heat transfer correlation for thermally developing laminar flow in a smooth tube with a twisted-tape insert, *International Journal of Heat and Mass Transfer*, 30(3) (1987) 509-515.
- [44] K.Y. Lim, Y.M. Hung, B.T. Tan, Performance evaluation of twisted-tape insert induced swirl flow in a laminar thermally developing heat exchanger, *Applied Thermal Engineering*, 121(Supplement C) (2017) 652-661.
- [45] W.M. Chakroun, S.F. Al-Fahed, The effect of twisted-tape width on heat transfer and pressure drop for fully developed laminar flow, *Journal of Engineering for Gas Turbines and Power*, 118(3) (1996) 584-589.
- [46] R.M. Manglik, A.E. Bergles, Characterization of twisted-tape-induced helical swirl flows for enhancement of forced convective heat transfer in single-phase and two-phase flows, *Journal of Thermal Science and Engineering Applications*, 5 (2013) 1-12.

- [47] R.M. Manglik, A.E. Bergles, Heat transfer and pressure drop correlations for twisted-tape inserts in isothermal tubes: Part II - transition and turbulent flows, *Journal of Heat Transfer*, 115(4) (1993) 890-896.
- [48] H. Bas, V. Ozceyhan, Optimization of Parameters for Heat Transfer and Pressure Drop in a Tube with Twisted Tape Inserts by Using Taguchi Method, *Arabian Journal for Science and Engineering*, 39(2) (2014) 1177-1186.
- [49] M.M.K. Bhuiya, A.S.M. Sayem, M. Islam, M.S.U. Chowdhury, M. Shahabuddin, Performance assessment in a heat exchanger tube fitted with double counter twisted tape inserts, *International Communications in Heat and Mass Transfer*, 50 (2014) 25-33.
- [50] A. Sroysroy, S. Eiamsa-ard, Periodically fully-developed heat and fluid flow behaviors in a turbulent tube flow with square-cut twisted tape inserts, *Applied Thermal Engineering*, 112 (2017) 895-910.
- [51] C. Man, C. Wang, J. Yao, The current situation of the study on twisted tape inserts in pipe exchangers, *Journal of Marine Science and Application*, 13(4) (2014) 477-483.
- [52] S. Liu, M. Sakr, A comprehensive review on passive heat transfer enhancements in pipe exchangers, *Renewable and Sustainable Energy Reviews*, 19 (2013) 64-81.
- [53] R.M. Manglik, A.E. Bergles, Swirl flow heat transfer and pressure drop with twisted-tape inserts, *Advances in Heat Transfer*, 36 (2002) 183-266.
- [54] A. Dewan, P. Mahanta, K.S. Raju, P.S. Kumar, Review of passive heat transfer augmentation techniques, *Proceedings of the Institution of Mechanical Engineers, Part A: Journal of Power and Energy*, 218(7) (2004) 509-527.
- [55] C. Maradiya, J. Vadher, R. Agarwal, The heat transfer enhancement techniques and their thermal performance factor, *Beni-Suef University Journal of Basic and Applied Sciences*, 7(1) (2017) 1-21.

- [56] J.P. Meyer, Heat transfer in tubes in the transitional flow regime, in: Proceedings of the 15th International Heat Transfer Conference IHTC-15, Kyoto, Japan, 2014, pp. 1-21.
- [57] J.P. Meyer, S.M. Abolarin, Heat transfer and pressure drop in the transitional flow regime for a smooth circular tube with twisted tape inserts and a square-edged inlet, International Journal of Heat and Mass Transfer, 117 (2018) 11-29.
- [58] J. Dirker, J.P. Meyer, D.V. Garach, Inlet flow effects in micro-channels in the laminar and transitional regimes on single-phase heat transfer coefficients and friction factors, International Journal of Heat and Mass Transfer, 77 (2014) 612-626.
- [59] A.J. Ghajar, L.M. Tam, Heat transfer measurements and correlations in the transition region for a circular tube with three different inlet configurations, Experimental Thermal and Fluid Science, 8 (1994) 79-90.
- [60] A.J. Ghajar, L.M. Tam, Flow regime map for a horizontal pipe with uniform wall heat flux and three inlet configurations, Experimental Thermal and Fluid Science, 10 (1995) 287-297.
- [61] H.K. Tam, L.M. Tam, A.J. Ghajar, Effect of inlet geometries and heating on the entrance and fully-developed friction factors in the laminar and transition regions of a horizontal tube, Experimental Thermal and Fluid Science, 44 (2013) 680-696.
- [62] L.M. Tam, A.J. Ghajar, Effect of inlet geometry and heating on the fully developed friction factor in the transition region of a horizontal tube, Experimental Thermal and Fluid Science, 15 (1997) 52-64.
- [63] M. Everts, J.P. Meyer, Heat transfer of developing flow in the transitional flow regime, in: Proceedings of the 1st Thermal and Fluid Engineering Summer Conference, TFESC ASTFE, New York City, USA, 2015, pp. 1-13.

- [64] J.P. Meyer, J.A. Olivier, Transitional flow inside enhanced tubes for fully developed and developing flow with different types of inlet disturbances: Part II-heat transfer, *International Journal of Heat and Mass Transfer*, 54(7-8) (2011) 1598-1607.
- [65] M. Everts, J.P. Meyer, Flow regime maps for smooth horizontal tubes at a constant heat flux, *International Journal of Heat and Mass Transfer*, 117 (2018) 1274-1290.
- [66] M. Everts, J.P. Meyer, Heat transfer of developing and fully developed flow in smooth horizontal tubes in the transitional flow regime, *International Journal of Heat and Mass Transfer*, 117 (2018) 1331-1351.
- [67] J.P. Meyer, M. Everts, A.T.C. Hall, F.A. Mulock-Houwer, M. Joubert, L.M.J. Pallent, E.S. Vause, Inlet tube spacing and protrusion inlet effects on multiple circular tubes in the laminar, transitional and turbulent flow regimes, *International Journal of Heat and Mass Transfer*, 118 (2018) 257-274.
- [68] M. Everts, J.P. Meyer, Relationship between pressure drop and heat transfer of developing and fully developed flow in smooth horizontal circular tubes in the laminar, transitional, quasi-turbulent and turbulent flow regimes, *International Journal of Heat and Mass Transfer*, 117 (2018) 1231-1250.
- [69] J.P. Meyer, M. Everts, Single-phase mixed convection of developing and fully developed flow in smooth horizontal circular tubes in the laminar and transitional flow regimes, *International Journal of Heat and Mass Transfer*, 117 (2018) 1251-1273.
- [70] C.O. Popiel, J. Wojtkowiak, Simple formulas for thermophysical properties of liquid water for heat transfer calculations (from 0°C to 150°C), *Heat Transfer Engineering*, 19(3) (1998) 87-101.
- [71] P.F. Dunn, *Measurement and data analysis for engineering and science*, 2nd ed., CRC Press, Taylor and Francis Group, Boca Raton, New York, USA, 2010.

- [72] S.M. Morcos, A.E. Bergles, Experimental investigation of combined forced and free laminar convection in horizontal tubes, *Journal of Heat Transfer*, 97 (1975) 212-219.
- [73] F.L. Test, Laminar flow heat transfer for fluids and liquids with temperature-dependent viscosity, *Journal of Heat Transfer*, 90 (1968) 385-393.
- [74] P.R.H. Blasius, The law of similarity of frictional processes in fluids. Originally in German: das aehnlichkeitsgesetz bei reibungsvorgangen in flüs sigk eiten, *ForschArbeitIngenieur-Wesen*, (131) (1913) 1-4.
- [75] R.W. Allen, E.R.G. Eckert, Friction and heat-transfer measurements to turbulent pipe flow of water ($Pr=7$ and 8) at uniform wall heat flux, *Journal of Heat Transfer*, 86(3) (1964) 301-310.
- [76] L.M. Tam, A.J. Ghajar, The unusual behavior of local heat transfer coefficient in a circular tube with a bell-mouth inlet, *Experimental Thermal and Fluid Science*, 16(3) (1998) 187-194.
- [77] S.M. Abolarin, J.P. Meyer, M. Everts, Heat transfer and pressure drop enhancement characteristics of peripheral u-cut twisted tape and ring inserts in the transitional flow regime, *International Journal of Heat and Mass Transfer*, Manuscript number: HMT_2018_4598. Status: Accepted on 8 December 2018. (2018).
- [78] A.W. Date, Prediction of fully-developed flow containing a twisted-tape, *International Journal of Heat and Mass Transfer*, 17 (1974) 845-859.
- [79] A. Pantokratoras, Steady laminar flow in a 90° bend, *Advances in Mechanical Engineering*, 8(9) (2016) 1-9.

List of figures

Fig. 1. Schematic representation of the experimental set-up.

Fig. 2. Schematic diagram (not to scale) showing (a) the test section with a CCCTT insert, the 21 measuring stations ($T_1 - T_{21}$) and location at which the bulk temperatures, T_b , was obtained, as well as the two pressure taps (P_1 and P_2) and (b) cross-sectional view of the test section with the four thermocouple positions on the periphery of the tube.

Fig. 3. Schematic representation of the CCCTT inserts with connection angles, θ , of (a) 0° , (b) 30° and (c) 60° , as well as photographs of the CCCTT inserts with connection angles of (d) 0° , (e) 30° and (f) 60° .

Fig. 4. Comparison of (a) Reynolds numbers uncertainties and (b) Colburn j -factors uncertainties as a function of Reynolds number at $x/D_i = 246$, as well as (c) friction factors uncertainties as a function of bulk Reynolds number of the CCCTT insert with the connection angle of 60° , CTT insert with twist ratio of 5 [57] and smooth tube, at a heat flux of 4 kW/m^2 . The “ L ”-values indicates the end of the laminar flow regimes and the transitional flow regime is indicated by ΔRe , therefore the laminar (L) and turbulent flow regimes are to the left and right of ΔRe respectively.

Fig. 5. Illustration of the linear line method [57] used to identify the three flow regimes for the heat transfer results as a function of Reynolds number at $x/D_i = 246$ a heat flux of 1.35 kW/m^2 and connection angle of 60° . The “ $L-L$ ”, “ $R-R$ ” and “ $T-T$ ” lines represent the laminar, transitional and turbulent flow regimes respectively.

Fig. 6. Comparison of (a) the Colburn j -factors as a function of local Reynolds number at $x/D_i = 246$, and (b) the friction factors as a function of bulk Reynolds number at $x/D_i = 198$, for the CTT insert [57], CCCTT insert with a connection angle of 60° and PUCTT22 insert

with depth ratio of 0.216 [77]. The experiments were conducted at a heat flux of 2 kW/m² and all tapes had a twist ratio of 5.

Fig. 7. Comparison of (a) Colburn j -factors as a function of local Reynolds number at $x/D_i = 246$ and (b) friction factors as a function of bulk Reynolds number at $x/D_i = 198$ for CCCTT inserts at the heat flux of 3 kW/m² and different connection angles.

Fig. 8. Comparison of (a) Colburn j -factors as a function of local Reynolds number at $x/D_i = 246$ and (b) friction factors as a function of bulk Reynolds number at $x/D_i = 198$, for CCCTT inserts with a connection angle of 30° and heat fluxes of 1.35, 2, 3 and 4 kW/m².

Fig. 9. Heat transfer and pressure drop results in terms of (a) $Re_{cr}(x)/[Gr^*(x)]^{0.416}$ to obtain the start of the transitional flow regime (Eq. 13) and (b) $Re_{qt}(x)/[Gr^*(x)]^{0.275}$ to obtain the end of the transitional flow regime (Eq. 14) as a function of $\cos\theta$.

Fig. 10. Heat transfer results as a function of Reynolds number to obtain Colburn j -factor correlations in the (a) laminar flow regime (Eq. 15), (b) transitional flow regime (Eq. 16) and (c) turbulent flow regime (Eq. 17) for different connection angles and heat fluxes.

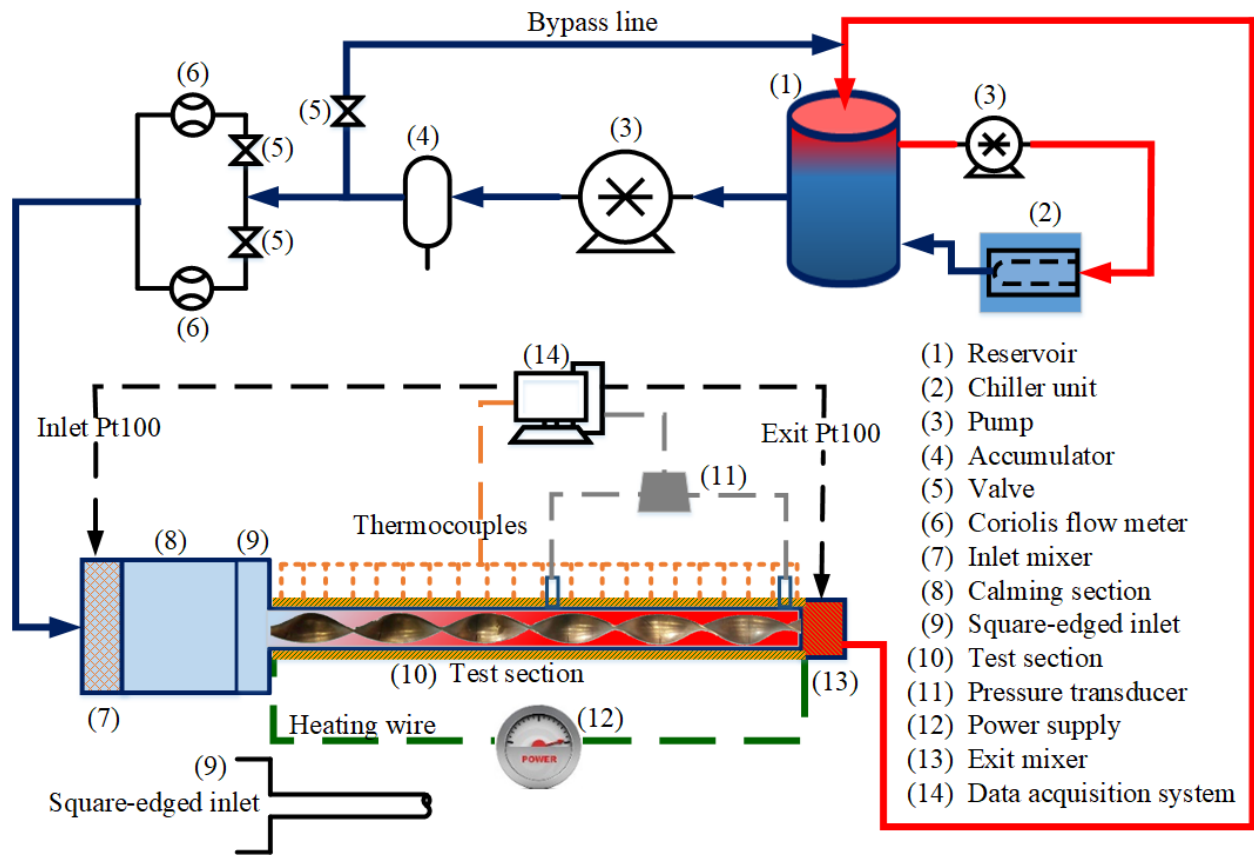


Fig. 1.

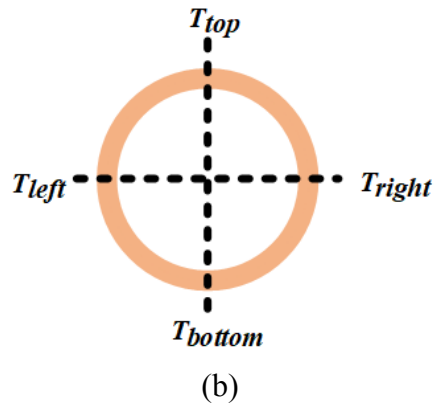
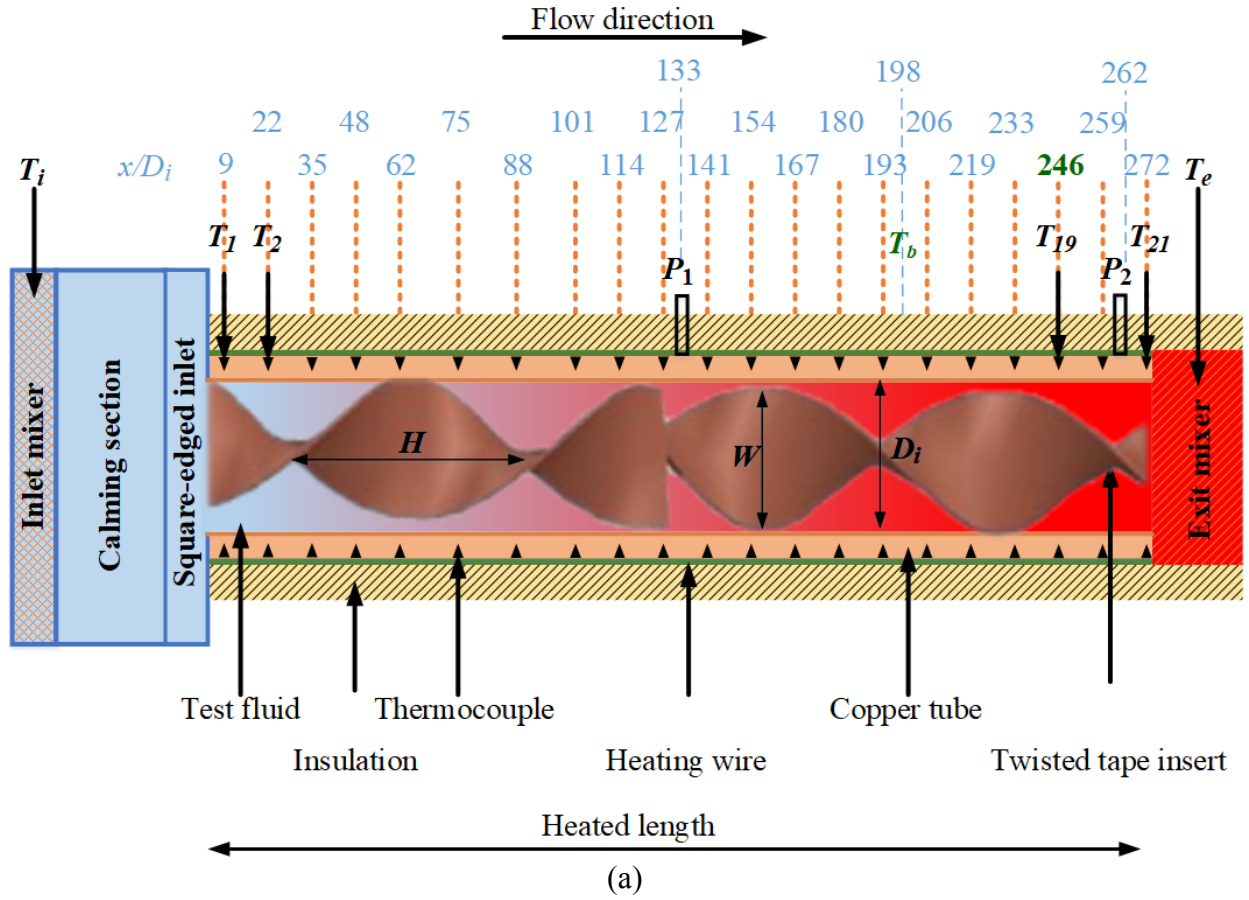


Fig. 2.

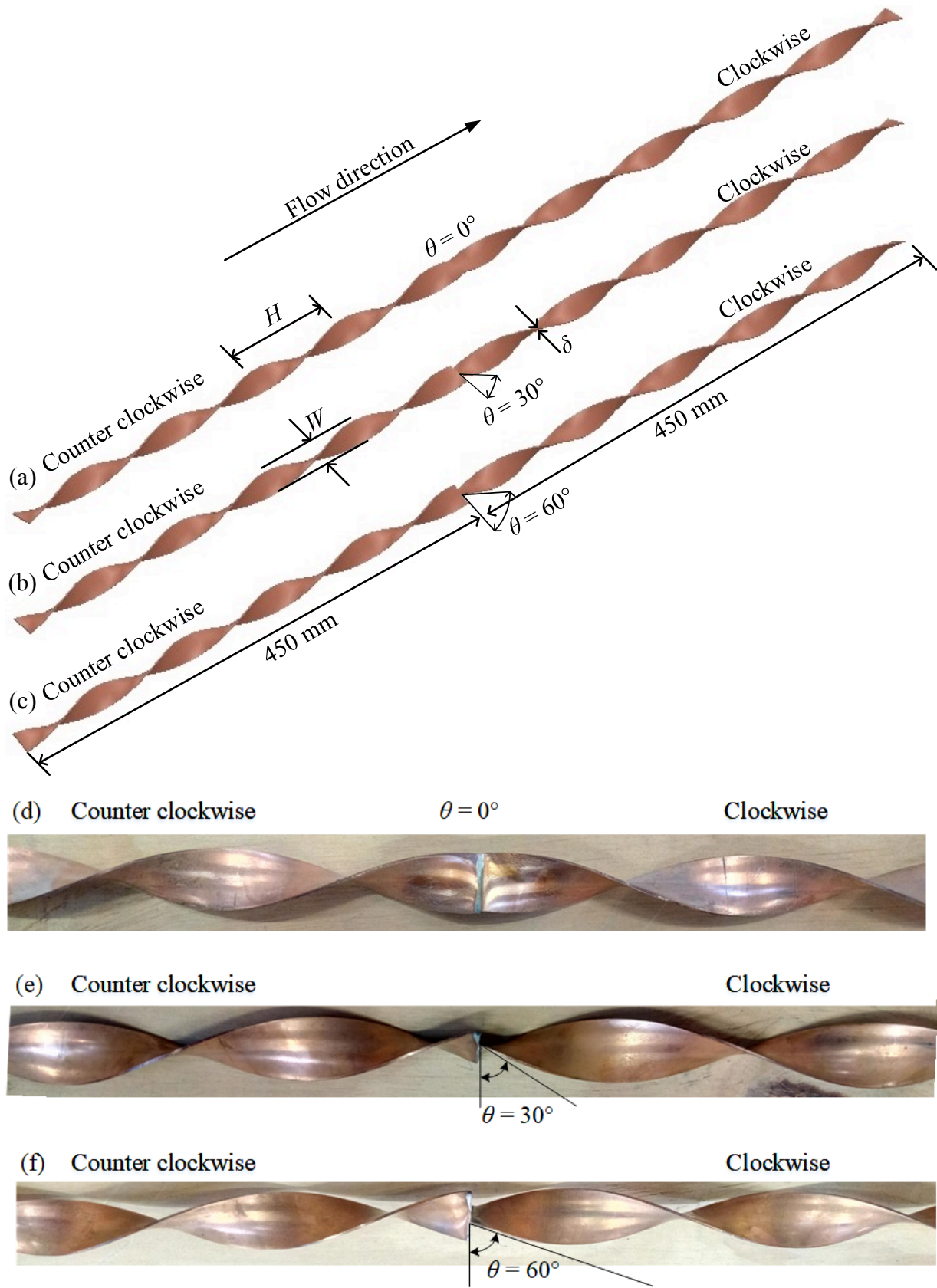
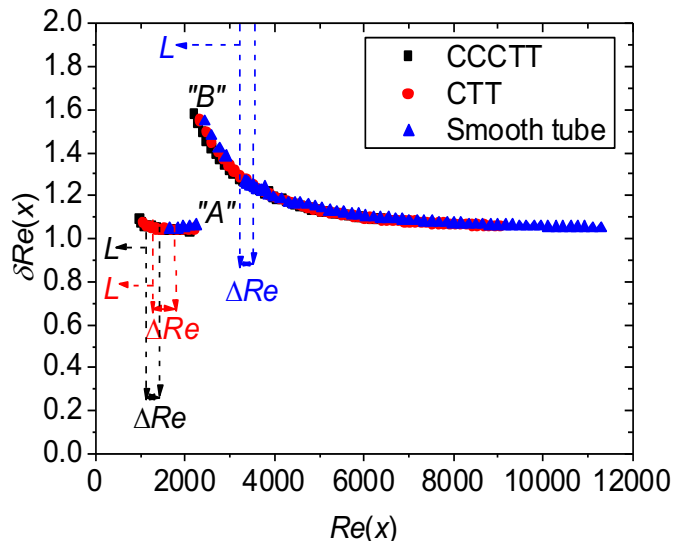
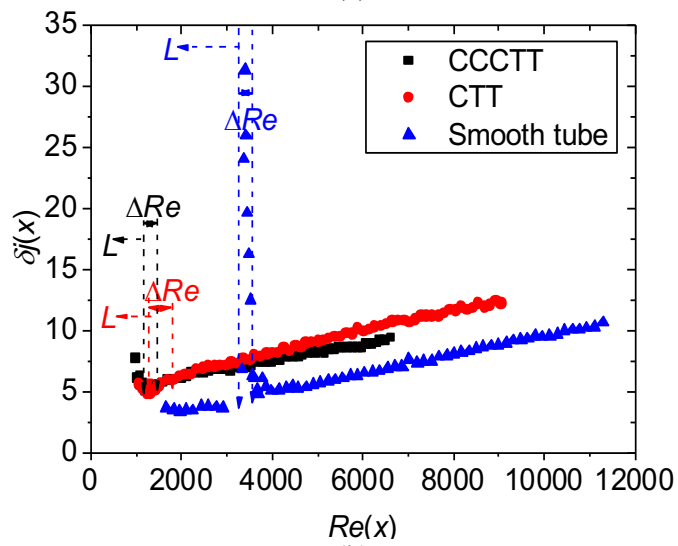


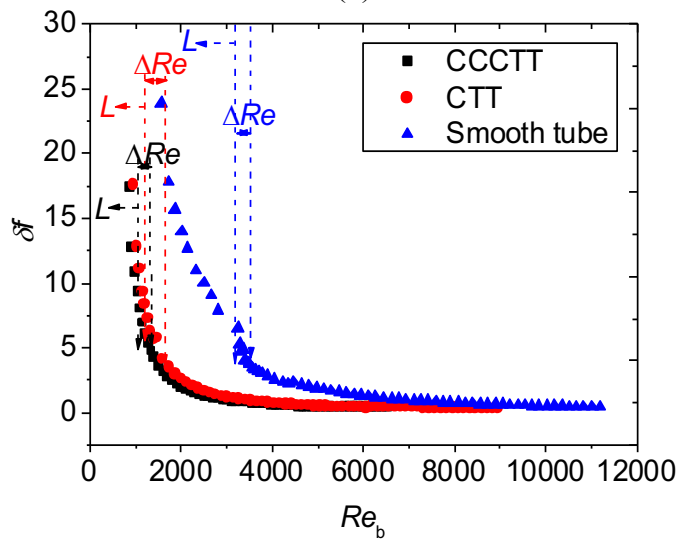
Fig. 3.



(a)



(b)



(c)

Fig. 4.

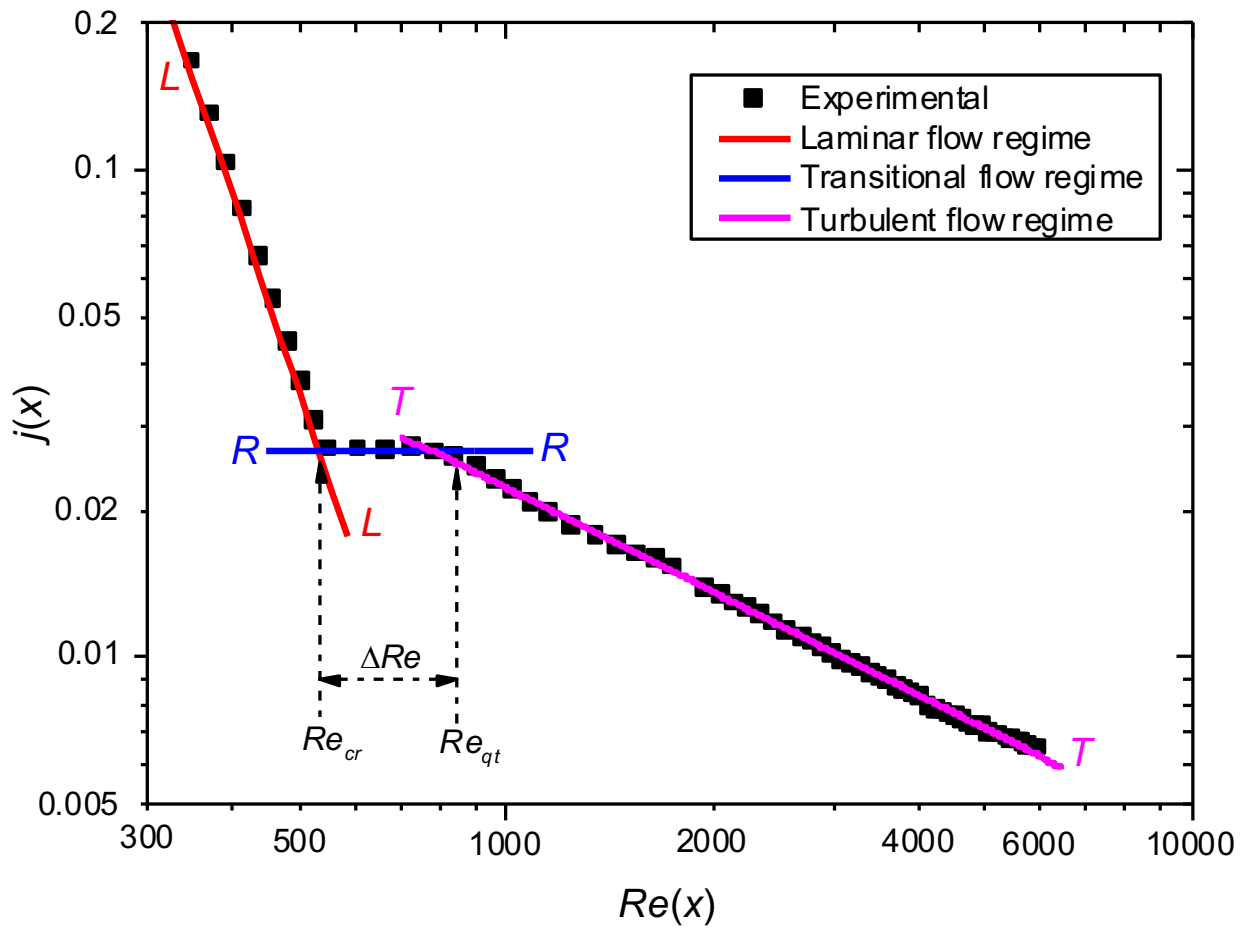
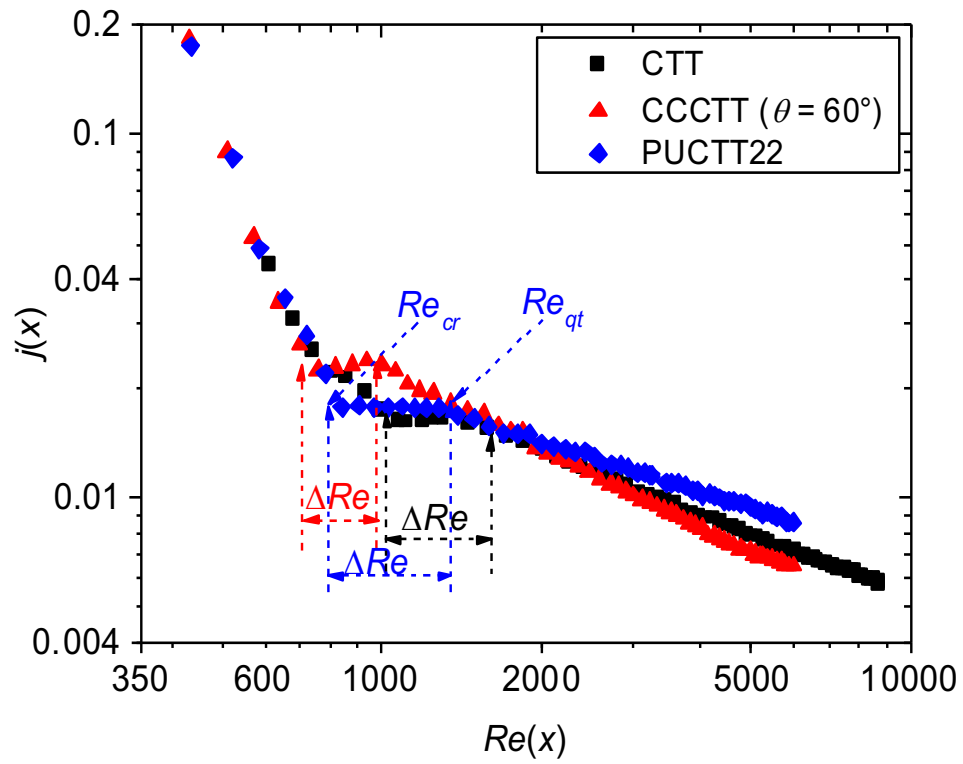
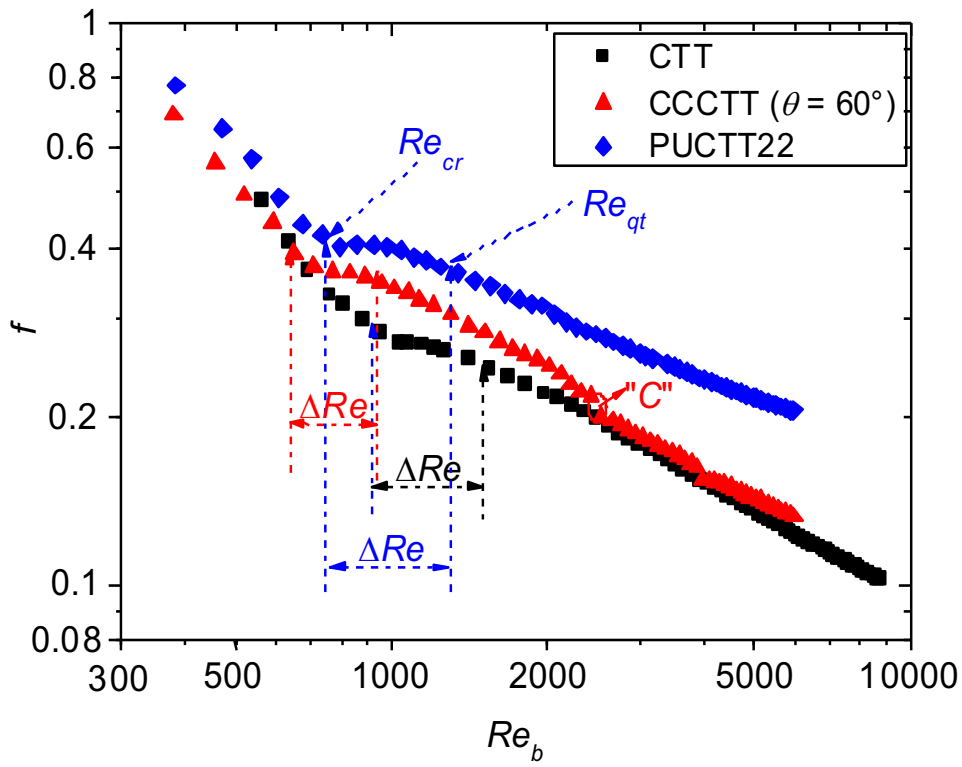


Fig. 5.



(a)



(b)

Fig. 6

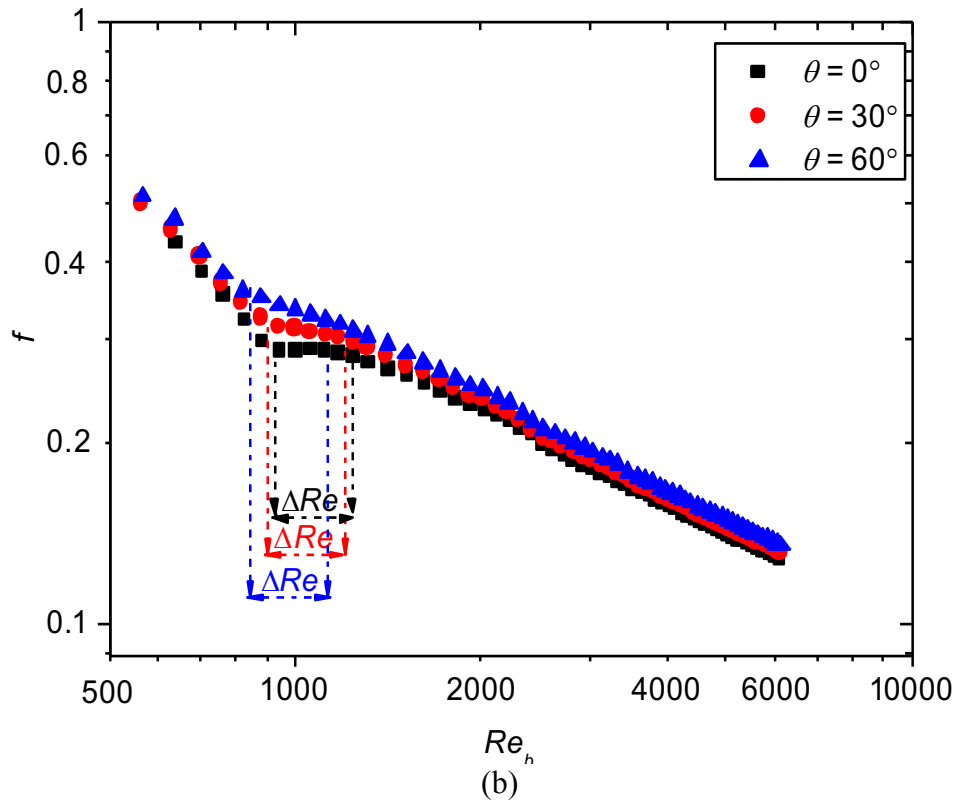
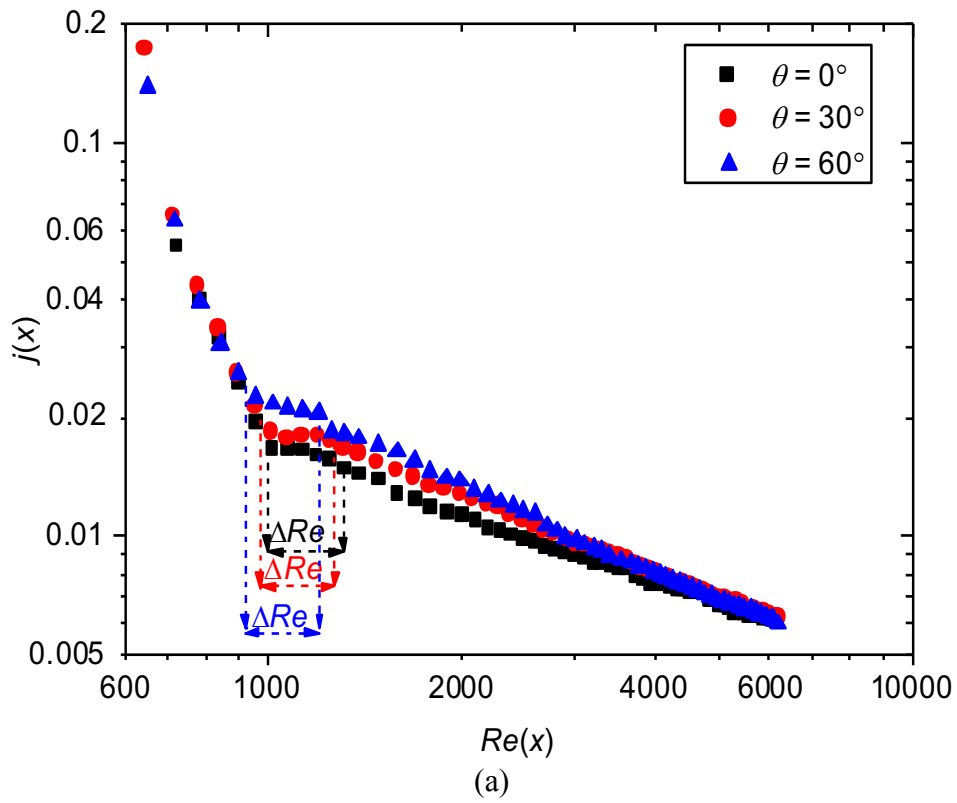


Fig. 7

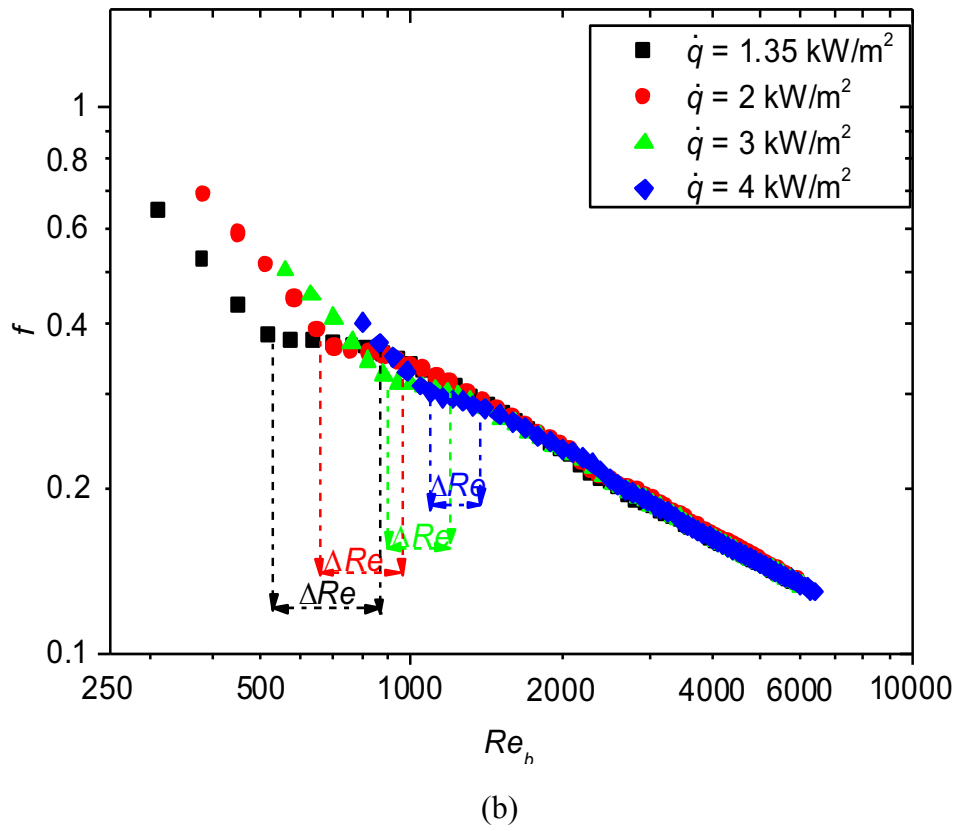
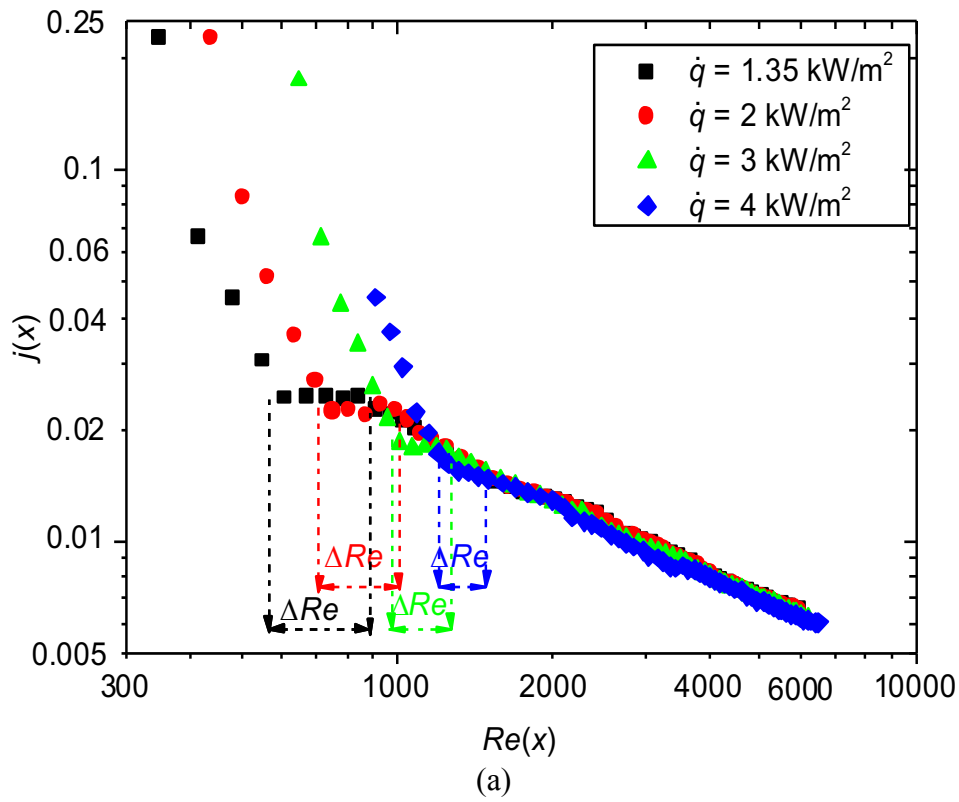


Fig. 8

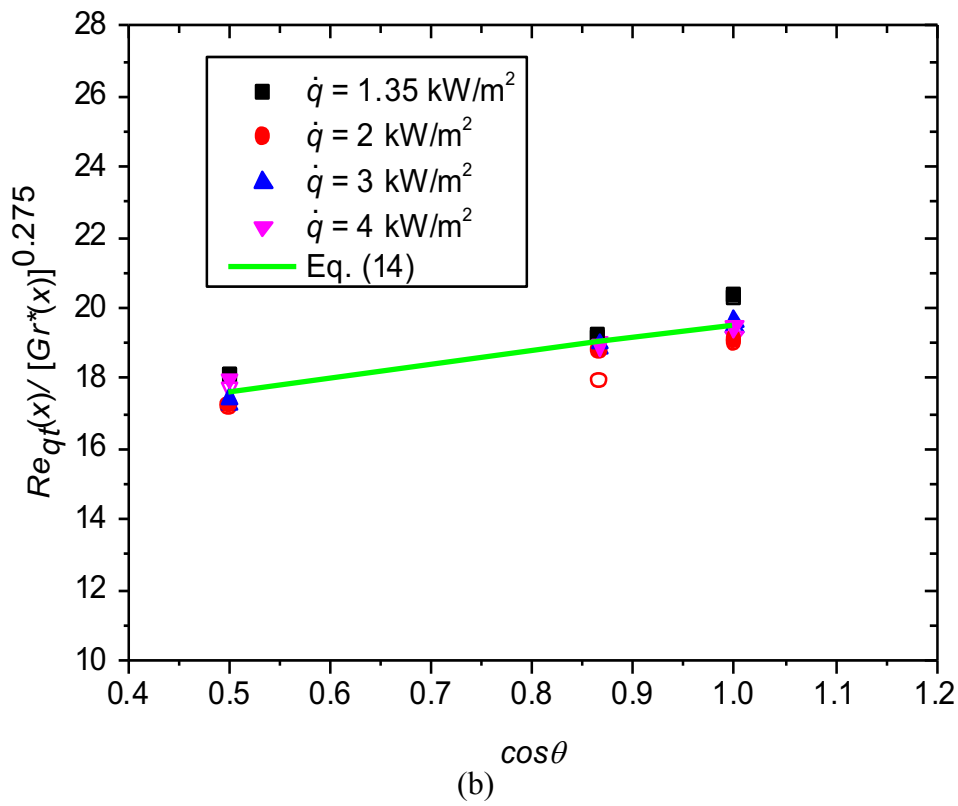
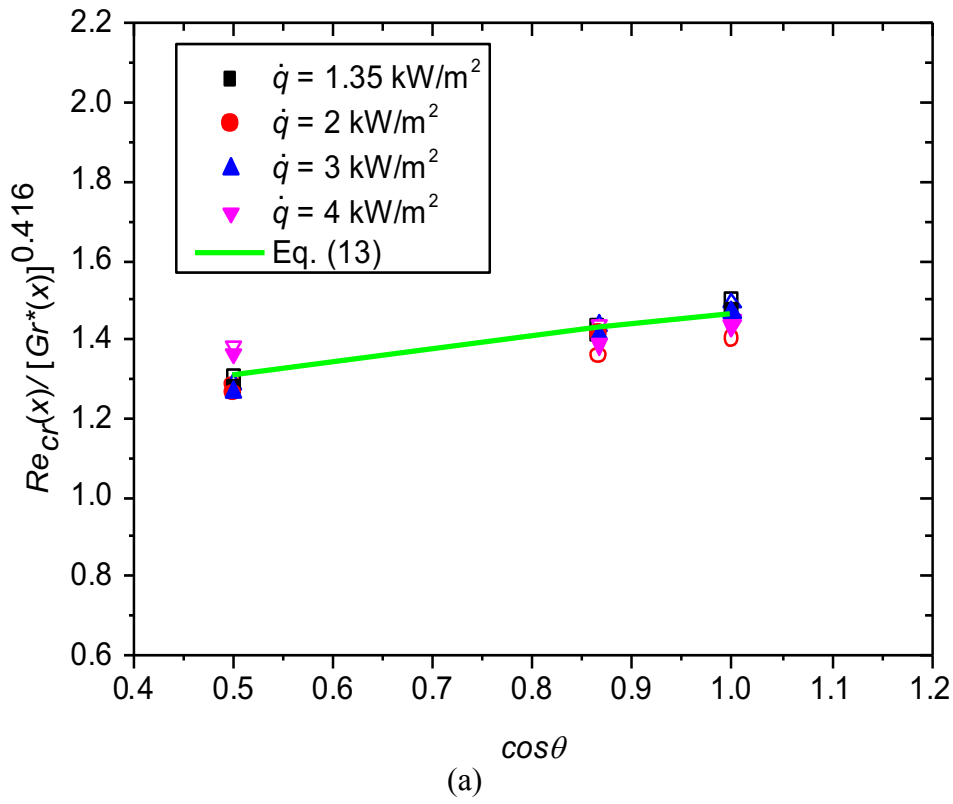


Fig. 9

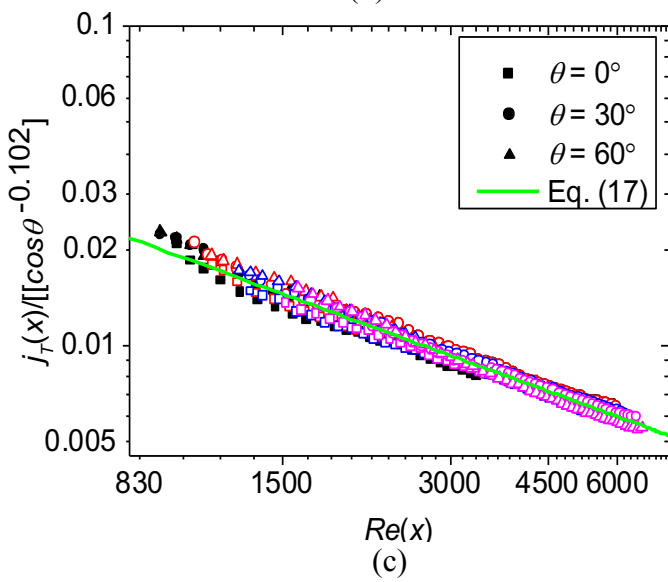
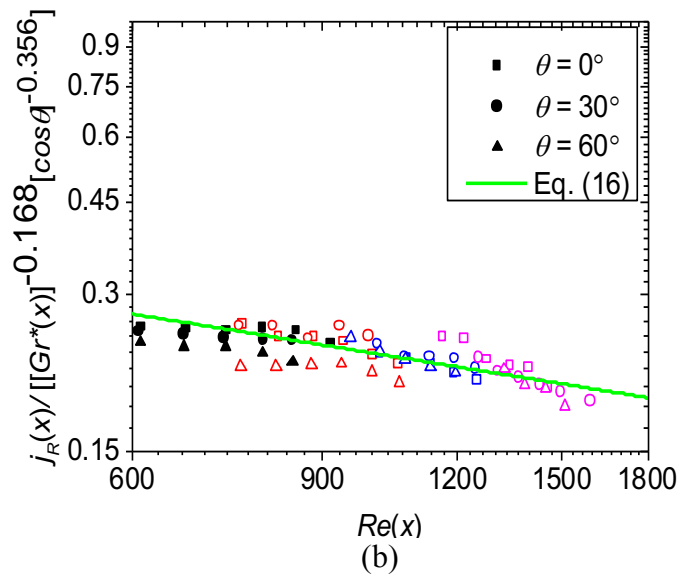
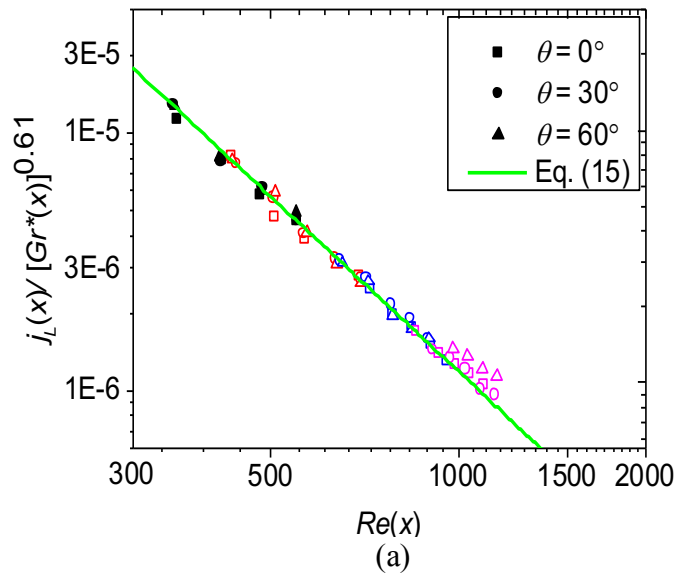


Fig. 10.

List of tables

Table 1: Ranges and accuracies of the experimental instrumentation.

Table 2: Parametric values of the experimental setup.

Table 3: Summary of the start, end and width of transitional flow regime for the Colburn j -factors and friction factors with CCCTT inserts.

Table 4: The ranges and performance of the Colburn j -factor (Section 7.4.2) and friction factor (Section 7.4.3) correlations of the CCCTT inserts.

Table 1

	Instrument	Range	Accuracy
Flow meters	CMF 010	0 – 108 ℓ/h	0.054 ℓ/h (0.05% of full scale)
	CMF 025	0 – 2 180 ℓ/h	1.09 ℓ/h (0.05% of full scale)
Thermocouples		<150 °C	0.1 °C
Pt100 probes		0 – 250 °C	0.06 °C
Power supplies	Current	0 – 15 A	0.2% of maximum value
	Voltage	0 – 360 V	0.2% of maximum value
Pressure transducers	0.86 kPa diaphragm	0 – 0.86 kPa	2.15 Pa (0.25% of full scale)
	1.4 kPa diaphragm	0 – 1.4 kPa	3.5 Pa (0.25% of full scale)

Table 2

Parameters	Symbols	Values
Outer diameter of test section	D_o	22.0 mm
Inner diameter of test section	D_i	19.0 mm
Heat transfer length	L_h	4.8 m
Pressure drop length	$L_{\Delta P}$	2.45 m
Thickness of twisted tape inserts	δ	1 mm
Pitch of the twisted tape inserts	H	90 mm
Length of twisted tape/test section	L	5.27 m
Width of twisted tape insert	W	18 mm
Twist ratio	y	5
Connection angles	θ	0°, 30° and 60°
Prandtl numbers	Pr	2.1 – 6.58
Heat fluxes	\dot{q}	1.35, 2, 3 and 4 kW/m ²
Reynolds number range for CCCTT	Re	300 – 6 675
Reynolds number range for the smooth tube	Re	1 331-11 404
Inlet temperature of the test fluid	T_i	20°C

Table 3:

Connection angle, θ	Symbols	Heat flux, \dot{q} [kW/m ²]							
		1.35	2	3	4	1.35	2	3	4
		Colburn j -factors, j				Friction factors, f			
0°	Re_{cr}	584	722	997	1 212	553	675	923	1 108
	Re_{qt}	948	1 055	1 308	1 502	917	1 010	1 237	1 404
	ΔRe	363	333	311	290	364	335	314	296
30°	Re_{cr}	563	705	973	1 184	532	657	898	1 082
	Re_{qt}	894	1 008	1 271	1 465	864	962	1 200	1 368
	ΔRe	331	303	298	281	332	305	302	286
60°	Re_{cr}	529	685	920	1 173	498	637	844	1 070
	Re_{qt}	847	978	1 200	1 413	818	932	1 127	1 314
	ΔRe	318	289	280	240	320	295	283	244

Table 4:

		Eq.	Average deviation [%]	Maximum deviation [%]	Range
Transitional flow regime boundaries	Re_{cr}	(13)	1	6	$533 \leq Re(x) \leq 1\,173$ $1.47 \times 10^6 < Gr^*(x) < 1.13 \times 10^7$ $0^\circ \leq \theta \leq 60^\circ$ $y = 5$
	Re_{qt}	(14)	0.1	6	$917 \leq Re(x) \leq 1\,413$ $1.03 \times 10^6 < Gr^*(x) < 7.78 \times 10^6$ $0^\circ \leq \theta \leq 60^\circ$ $y = 5$
Colburn j -factors	Laminar	(15)	3	12	$300 < Re(x) < 1\,200$ $1.83 \times 10^6 < Gr^*(x) < 3.2 \times 10^7$ $0^\circ \leq \theta \leq 60^\circ$ $y = 5$
	Transitional	(16)	3	13	$600 < Re(x) < 1\,500$ $1.18 \times 10^6 < Gr^*(x) < 1.2 \times 10^7$ $0^\circ \leq \theta \leq 60^\circ$ $y = 5$
	Turbulent	(17)	2	13	$900 < Re(x) < 6\,600$ $8 \times 10^5 < Gr^*(x) < 7.13 \times 10^6$ $0^\circ \leq \theta \leq 60^\circ$ $y = 5$
Friction factors	Laminar	(18)	5	17	$300 < Re_b < 1\,200$ $1.52 \times 10^6 < Gr_b^* < 2.3 \times 10^7$ $0^\circ \leq \theta \leq 60^\circ$ $y = 5$
	Transitional	(19)	2	10	$570 < Re_b < 1\,400$ $1.06 \times 10^6 < Gr_b^* < 9.26 \times 10^6$ $0^\circ \leq \theta \leq 60^\circ$ $y = 5$
	Turbulent	(20)	1	8	$878 < Re_b < 6\,400$ $7.54 \times 10^5 < Gr_b^* < 5.86 \times 10^6$ $0^\circ \leq \theta \leq 60^\circ$ $y = 5$